


# Deciphering post-caldera volcanism: insight into the Vulcanello (Island of Vulcano, Southern Italy) eruptive activity based on geological and petrological constraints

Raffaella Fusillo<sup>1</sup> · Federico Di Traglia<sup>2</sup> · Anna Gioncada<sup>3</sup>  · Marco Pistolesi<sup>2</sup> · Paul J. Wallace<sup>4</sup> · Mauro Rosi<sup>3</sup>

Received: 16 May 2015 / Accepted: 26 July 2015 / Published online: 9 August 2015  
© Springer-Verlag Berlin Heidelberg 2015

**Abstract** Integrated field-based volcanology and petrologic studies can provide relevant clues about the way in which structural features, magma replenishment of a shallow subcaldera reservoir, and magma evolution exert control on eruption behavior during post-caldera volcanism. Post-caldera activity of the past 1000 years at the La Fossa caldera (Island of Vulcano, Italy) occurred at two vents: the dominantly explosive La Fossa vent located at the center of the caldera and the lava-dominated Vulcanello vent located close to the northern ring fault of the caldera. Revised chrono-stratigraphic data indicate that the activity occurred in two clusters of eruptions: in the eleventh to twelfth centuries and during the seventeenth century. The activity was, in part, contemporaneous with La Fossa vent and led to the formation of three, partially overlapped Strombolian cones. Each cone-building episode was accompanied by the outpouring of lava in subaerial and submarine environments. The erupted volumes of the pyroclastic cones vary between  $2 \times 10^{-3}$  and  $3 \times 10^{-6}$  km<sup>3</sup>, while the volumes of the three lavas span

between 0.3 km<sup>3</sup> (a submarine lava field) and  $3 \times 10^{-3}$  km<sup>3</sup>. Petrology data indicate that the activity of Vulcanello was fed by three different magma batches: Vulcanello 1 was fed by a slightly zoned reservoir of shoshonitic composition, Vulcanello 2 was fed by a slightly more evolved magma whereas Vulcanello 3 was fed by latitic magma. The compositions of melt inclusions (major elements and volatile content) trapped in olivine separated from pyroclastic materials record the entire differentiation history and suggest that all Vulcanello magmas underwent volatile loss during pre-eruption equilibration at  $\leq 1$  km depth. Integration of all available information also suggests that in the last 1000 years, the northern caldera fault acted as a preferential duct for the rise of degassed magma from the sub-caldera magma reservoir whereas volatile release namely took place separately at La Fossa cone where activity was almost entirely explosive in nature.

**Keywords** Post-caldera volcanism · Melt inclusions · Shoshonitic volcanism · Aeolian archipelago

Editorial responsibility: S. Calvari

**Electronic supplementary material** The online version of this article (doi:10.1007/s00445-015-0963-6) contains supplementary material, which is available to authorized users.

✉ Anna Gioncada  
gioncada@dst.unipi.it

<sup>1</sup> Department of Earth Sciences, University of Bristol, Wills Memorial Building, Queen's Road, BS8 1RJ Bristol, UK

<sup>2</sup> Dipartimento di Scienze della Terra, Università di Firenze, Via La Pira 4, 50121 Florence, Italy

<sup>3</sup> Dipartimento di Scienze della Terra, Università di Pisa, Via Santa Maria 53, 56126 Pisa, Italy

<sup>4</sup> Department of Geological Sciences, University of Oregon, Eugene, OR 97403, USA

## Introduction

Post-caldera volcanism reflects the evolution of residual magma evolution and/or magma chamber replenishment episodes in the period following caldera collapse (Druitt et al. 2012), and it is generally controlled by the geometric and kinematic features of ring faults (Geyer and Marti 2014).

This work is aimed at understanding magma intrusion and migration leading to the onset of the eruptive activity at post-caldera volcanoes. We choose as a case study the Vulcanello peninsula, a ring fault volcano located in the northern part of La Fossa caldera (Island of Vulcano; Fig. 1), by analyzing the stratigraphic sequence along with geomorphologic and petrological studies.

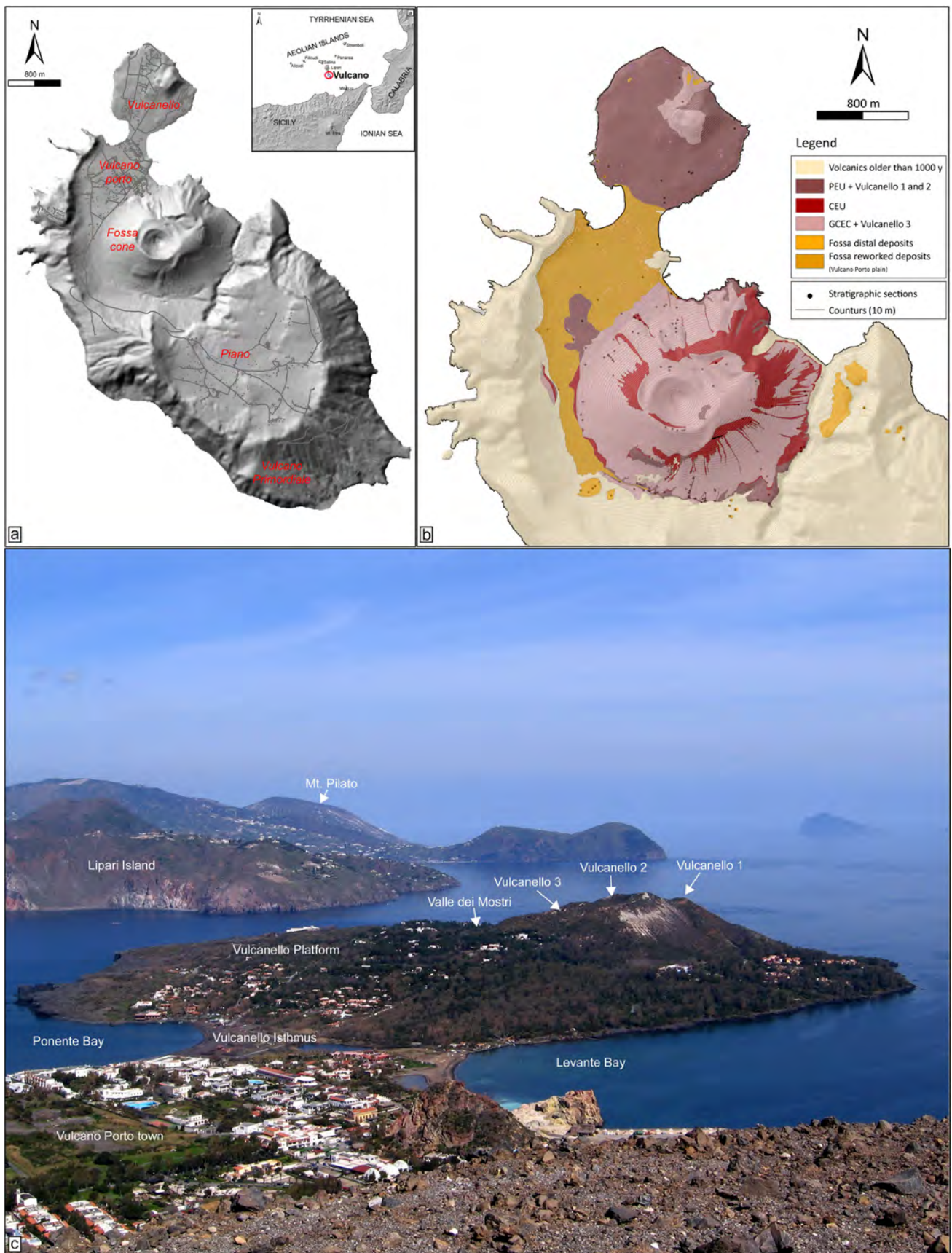


**Fig. 1** **a** The island of Vulcano. **b** Geology of Vulcano modified after Di Traglia et al. (2013). **c** Vulcanello peninsula (view from La Fossa)

## Geological setting

The Island of Vulcano (Aeolian Islands, Southern Italy) consists of several volcanic edifices whose formation overlapped in time and space beginning 120 ka (Keller 1980; Lanza and Zanella 2003; De Astis et al. 2013 and references therein). The composite volcanic system comprises the Primordial Vulcano edifice (120–100 ka), dissected by the development of Il Piano caldera around 100 ka and subsequently by the La Fossa caldera (80 to 15 ka) (Keller 1980; Gioncada and Sbrana 1991). Over the past 15 ka, in the northern sector of the island (Keller 1980), several vents were activated in a N–S direction (Saraceno, La Fossa cone, Faraglione, Vulcanello). This alignment can also be traced toward the near Lipari island, which was characterized, in some cases, by contemporaneous volcanic activity (Gioncada et al. 2003; Forni et al. 2013). The two most recent volcanoes are La Fossa, a 391-m-high active composite cone that began to erupt around 5.5 ka according to Frazzetta et al. (1984), and Vulcanello, a small volcanic peninsula to the north (Fig. 1). The Vulcanello peninsula, a 123-m-high composite edifice showing three coalescent crater rims, is composed of a lava platform and three partially

overlapping scoria cones aligned NE–SW along the northern ring fault of La Fossa caldera (Ventura et al. 1999; Blanco-Montenegro et al. 2007; Davi et al. 2009; De Astis et al. 2013; Romagnoli et al. 2013). Vulcanello erupted shoshonitic to latitic products, with latite characterizing the last cycle of activity (Keller 1980; De Astis et al. 1997; Davi et al. 2009).

The onset of the Vulcanello activity is still a matter of debate. Some authors (Keller 1970, 1980; Voltaggio et al. 1995; De Astis et al. 2013) suggest that the early activities of Vulcanello may have occurred in 126 or 183 BC, as reported by the Strabo and Plinius historical chronicles quoted by Mercalli and Silvestri (1891) and De Fiore (1922), mainly based on radiometric ages and on the presence of the AD 776 M. Pilato tephra layer from Lipari Island above the Vulcanello lava platform (Keller 1980; De Astis et al. 2013) (Table 1). By contrast, Arrighi et al. (2006), based on archaeomagnetic studies, suggest that the Vulcanello lava platform was built up during a continuous volcanic activity which occurred from AD 1100 to 1250 (Table 1). This latter hypothesis is also supported by recent studies (Tanguy et al. 2003; Zanella 2006; Davi et al. 2009; Gurioli et al. 2012; Di Traglia et al. 2013), evidencing that the exotic tephra layer from the Island of

**Table 1** Synthesis of the direct and indirect (i.e., based on the exotic rhyolitic tephra of Pilato and Rocche Rosse eruptions at Lipari) geochronological constraints for the age of Vulcanello eruptions

	Pilato tephra	Vulcanello platform	Rocche Rosse tephra	Vulcanello 3
Mercalli and Silvestri (1891) historical records		183-126-91 BC, early emersion		
De Fiore (1922) historical records		183-126-91 BC		
Keller (1970), $^{14}\text{C}$ dating	1220±100 BP, paleosol	183-126-91 BC		325±100 years BP, paleosol
Keller (1980)		183-126-91 BC		
Voltaggio et al. (1995) $^{226}\text{Ra}/^{230}\text{Th}$ dating		1.9±0.2 kyear		
Keller (2002), $^{14}\text{C}$ dating	AD 776 (+110/−90)			
Tanguy et al. (2003) archeomagnetic data			AD 1220±30 (Rocche Rosse lava)	
Lanza and Zanella (2003) paleomagnetic data		1.9±0.1 ka		
Arrighi et al. (2006) archeomagnetic data [based on secular variation of the geomagnetic field reconstructed from Italian Lavas; Tanguy et al. 2003]		AD 1180±30 AD 1050±70 AD 1080±50 AD 1000±60 AD 1180±70 AD 1230±30 AD 1100±60		
Caron et al. (2012) $^{14}\text{C}$ dating			0.61±0.02 cal ka BP (cryptotephra in deep-sea core)	
Gurioli et al. (2012) archeomagnetic data [based on French secular variation curve; Gallet et al. 2002]			AD 918–1302 (Breccia di Commenda lithic clasts)	

Lipari overlying the Vulcanello lava platform can be attributed to the explosive phase of the Rocche Rosse eruption (the Rocche Rosse tephra, Cortese et al. 1986; Dellino and La Volpe 1995) representing the most recent phases of activity on Lipari (AD 1220). Forni et al. (2013) suggest that on Lipari island, the Rocche Rosse, included within the Vallone Fiume Bianco Synthem, was characterized by a complex sequence of explosive phases that mostly produced a succession of fallout, lithic-rich pumiceous lapilli tuffs, with minor interlayered beds of lapilli tuffs with accretionary lapilli deposited from dilute pyroclastic density currents which heralded the emission of a final lava coulee. Archeomagnetic dating on the coulee (Tanguy et al. 2003) and fission track age (Bigazzi et al. 2003) on a coeval pyroclastic sequence (Lami succession) suggest the AD 1220 as the most probable age for the Rocche Rosse eruptive sequence. In agreement, the Rocche Rosse tephra was found on Vulcano island interbedded with the Breccia di Commenda eruption deposit (Gurioli et al. 2012; Di Traglia et al. 2013), dated using paleomagnetic methods on lithic clast by Gurioli et al. (2012) at AD 918–1302, and thus consistent with the AD 1230±40 archeomagnetic dating of Arrighi et al. (2006) of the Vulcanello platform and with the 0.61±0.02 cal ka BP (ca. AD 1335) <sup>14</sup>C dating of Caron et al. (2012) on cryptotephra found in a marine core from the Northern Ionian Sea.

Recently, a new stratigraphic reconstruction of the volcanoclastic succession of the last 1000 years of activity at La Fossa (Di Traglia et al. 2013) subdivided the stratigraphic record into two main units, namely the Palizzi–Commenda (PCEC) and Gran Cratere (GCEC) eruptive clusters. The eruptive cluster (EC) represents a series of eruptions clustered in time and forming a stratigraphic unit that is hierarchically higher than an eruptive unit but lower than an eruptive epoch (de Rita et al. 1998; Di Traglia et al. 2013); it is defined as a unit that is bounded by unconformities (erosional surfaces and/or palaeosols) and extends over a wide area (at least the cone and the surrounding plains and valleys). The oldest eruptive cluster (PCEC), comprising the Palizzi (PEU) and Commenda (CEU) eruptive units, occurred in the thirteenth century according to ages from Arrighi et al. (2006) and Gurioli et al. (2012), in a very short time compared to previous reconstructions. Archeomagnetic age and the identification of the Rocche Rosse tephra and the Pal B rhyolitic layer related to the PEU on top of the Vulcanello platform agree well with the onset of subaerial activity of Vulcanello close in time to the reactivation of the La Fossa cone in the late Middle Ages (~AD 1200) (Arrighi et al. 2006; Gurioli et al. 2012; Di Traglia et al. 2013; Table 1).

A larger consensus exists for timing of the products related to the last explosive activity (Vulcanello 3) emplaced above a paleosol dated at 0.397±0.097 ka (i.e., seventeenth century; Keller 1980). The isthmus linking Vulcanello and the rest of

Vulcano island (Vulcano Porto plain; Fig. 1) began to develop after the emplacement of the Vulcanello lava platform (post-twelfth century AD; Arrighi et al. 2006; Di Traglia et al. 2013).

## Data

Field data collection was carried out during different surveys starting from 2008. Forty natural sections were integrated with six machine-excavated and hand-dug pit trenches (Fig. 2). Morphological analysis and volume calculations for the Vulcanello peninsula were performed by integrating direct field observations with data from the DTM. Major element compositions of the juvenile clasts and volatile concentrations of olivine-hosted melt inclusions (MIs) were measured in quenched products of Vulcanello explosive activity. We also analyzed glass samples from the submarine effusive activity NE of Vulcanello (pillow lava). Methodological techniques are detailed in the [electronic supplementary material](#).

## Stratigraphy and eruptive units

The entire stratigraphic sequence of Vulcanello activity has been divided into three lithosomes (Vulcanello 1, Vulcanello 2, and Vulcanello 3); a comparison with previous reconstructions is shown in Table 2. A lithosome is an informal stratigraphic unit defined by lithological and morphological elements having a combination that defines a genetically homogeneous rock body, corresponding to a well-defined volcanic edifice with a recognizable morphology related to a defined eruptive centre (Giordano et al. 2006). In a map, a lithosome defines a stratigraphically and morphologically recognizable volcanic center (Tibaldi 2010). Each lithosome, which also marks a change of eruptive vent, is separated by erosive unconformities (e.g., the unconformable basal contact of a volcanic pile, the structural–morphological surface resulting from a caldera collapse) that are linked genetically to the evolution of the volcano (Palladino et al. 2010). Different from other stratigraphic units, lithosomes do not imply any hierarchic degree (Palladino et al. 2010). Within each lithosome, several eruptive (comprising both lavas and pyroclastic deposits) and epiclastic units (comprising deposits not directly related to eruptions; Manville et al. 2009) have been identified, separated by unconformities of lower rank compared to those between the lithosomes. Eleven EUs and three epiclastic units have been recognized: five EUs and two epiclastic units within Vulcanello 1, one EU and one epiclastic unit within Vulcanello 2, and six eruptive units within Vulcanello 3.

A synthetic log of the tephra units and lava flow deposits identified in the Vulcanello area and studied in this work (Fig. 3; Table 3) integrates the tephra sequence observed on the cones and on the lava plateau. The stratigraphic

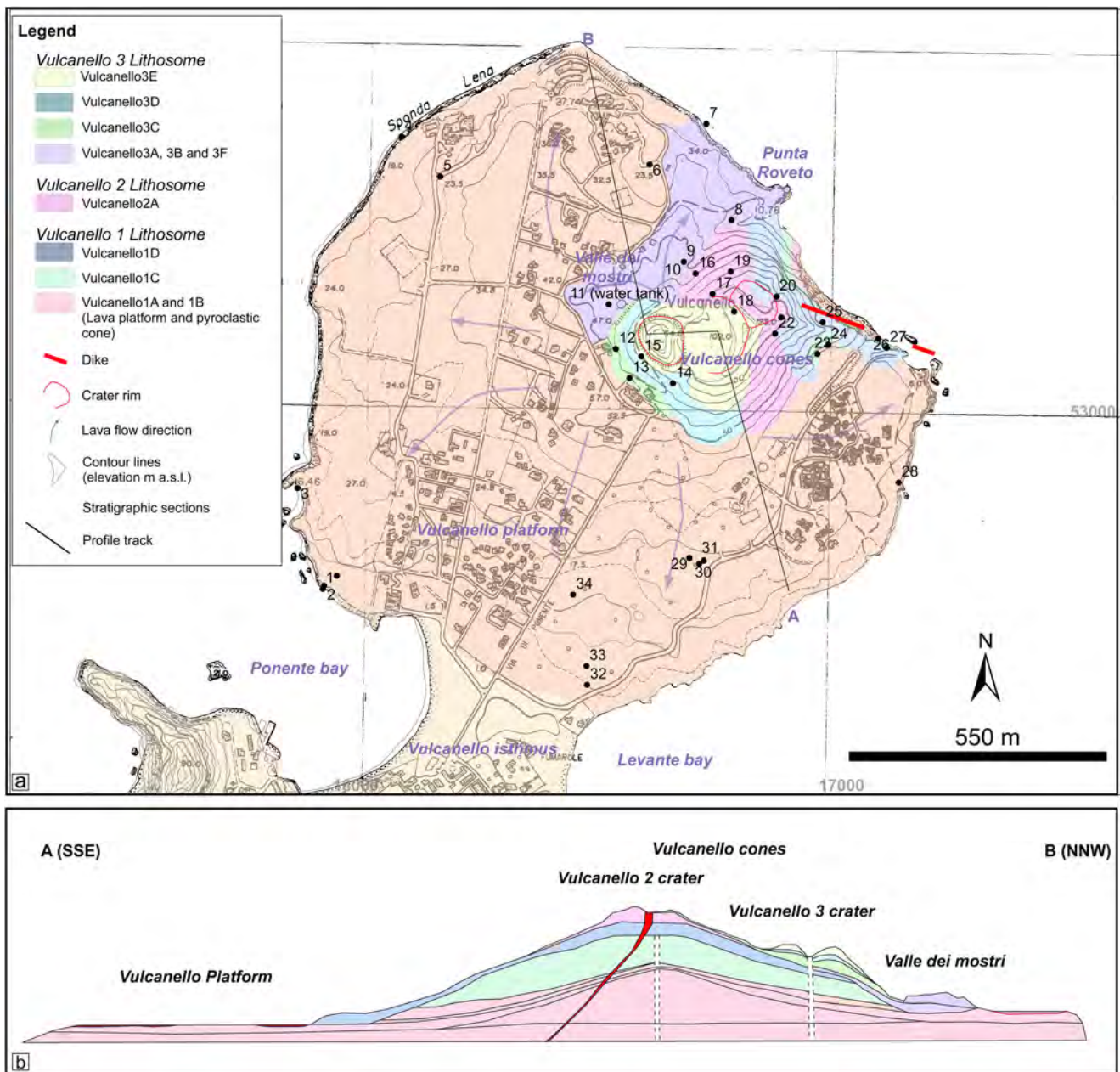


**Fig. 2** a Geology of Vulcanello peninsula from the new geological survey at 1:10,000 scale. b Cross section along the line A–B

relationships between Vulcanello deposits and La Fossa and Rocche Rosse (Lipari) deposits on the Vulcanello platform are exemplified in Fig. 4, using logs of selected natural outcrops and machine-excavated and hand-dug pit trenches.

*Vulcanello 1 lithosome*

We identified five EUs which correspond to the stratigraphic sequence of Vulcanello 1 lithosome. The Vulcanello 1A Unit is characterized by two different lithofacies (the plateau lava and the gray pyroclastics, Table 3, Fig. 5a, b). The plateau lava (Fig. 5a) is composed by several massive lava flows, often showing columnar jointing and ropy pahoehoe surfaces. The

gray pyroclastics are well exposed at the sea cliff in the eastern side (outcrops 26, 27 in Fig. 2) of the Vulcanello 1 cone, where they form a 9-m-thick, grain-supported, massive to stratified deposit. A 50-cm-thick volcanoclastic unit overlies the Vulcanello 1A deposits, indicating a short eruptive rest. This unit is, in turn, overlain by a massive lapilli deposit (Vulcanello 1B); on the eastern side of the cones (outcrops 26, 27 in Fig. 2), Vulcanello 1B is represented by a 3-m-thick, greenish, grain-supported, fine to coarse lapilli, normal to reversely graded deposit. A thin (15 cm) volcanoclastic unit separates Vulcanello 1B from Vulcanello 1C, which, in turn, outcrops in the eastern and southern side of the cones (outcrops 23, 24, 26, 27 in Fig. 2) as a 5-m-thick, normally graded,

**Table 2** Synoptic table comparing the stratigraphic reconstruction proposed in this work for Vulcanello, using lithosomes and eruptive units, with the previous reconstructions by Keller (1980), De Astis et al. (2013) and Di Traglia et al. (2013)

Keller (1980)	De Astis et al. (2006, 2013)	Di Traglia et al. (2013)	This work	
			Lithosome	Units
Structural units	Formations	Units		
Vulcanello 3	Vulcanello 3b (pyroclastics)	Vulcanello 3 (comprising Roveto lava flow)	Vulcanello 3	Vulcanello 3F (Valle dei Mostri lava flow) Vulcanello 3E Vulcanello 3D
Roveto lava flow	Vulcanello 3a (Roveto lava flow)			Vulcanello 3C Vulcanello 3B (Roveto lava flow) Vulcanello 3A
Lava platform	Vulcanello 2	Vulcanello 2	Vulcanello 2	Vulcanello 2
Vulcanello 2	Vulcanello 1b (lava platform)	Vulcanello 1 (comprising lava platform)	Vulcanello 1	Vulcanello 1D Vulcanello 1C Vulcanello 1B
Vulcanello 1	Vulcanello 1a (pyroclastics)			Vulcanello 1A (lava platform and pyroclastic cone)

lapilli to bomb-sized deposit. A 9-m-thick spatter deposit (Vulcanello 1D, Fig. 5c) closes the Vulcanello 1 lithosome. The entire stratigraphic sequence is cut by a feeding dike observable within the eastern sea cliff (Fig. 5b).

#### *Vulcanello 2 lithosome*

A time break between Vulcanello 1 and the overlying Vulcanello 2 lithosome is marked by a stratigraphic erosional unconformity and by the presence of a reworked deposit (maximum thickness 2 m; Fig. 6a). Vulcanello 2 is composed of a single EU (Vulcanello 2, Table 3), which outcrops on the northeastern cliff (outcrop 26 in Figs. 2a and 4) and in the southern flank of the cones (outcrop 22 in Fig. 2), where it forms a 3-m-thick fallout deposit characterized by a lower massive part grading upward into a normal-reversely graded deposit (Fig. 6a). The explosive activity of Vulcanello 2 is possibly associated with the intrusion of the dike that cuts all the products of Vulcanello 1 and with the emplacement a submarine lava field offshore of the northeastern side of Vulcanello (Gamberi et al. 1997; Gamberi 2001; Romagnoli et al. 2013).

Vulcanello 1 and Vulcanello 2 lithosomes are covered by the Pal B rhyolitic layer (Figs. 6 and 7), by the Rocche Rosse tephra (Fig. 8) and by the ash fraction of the Commenda deposit (Figs. 7, 8, and 9).

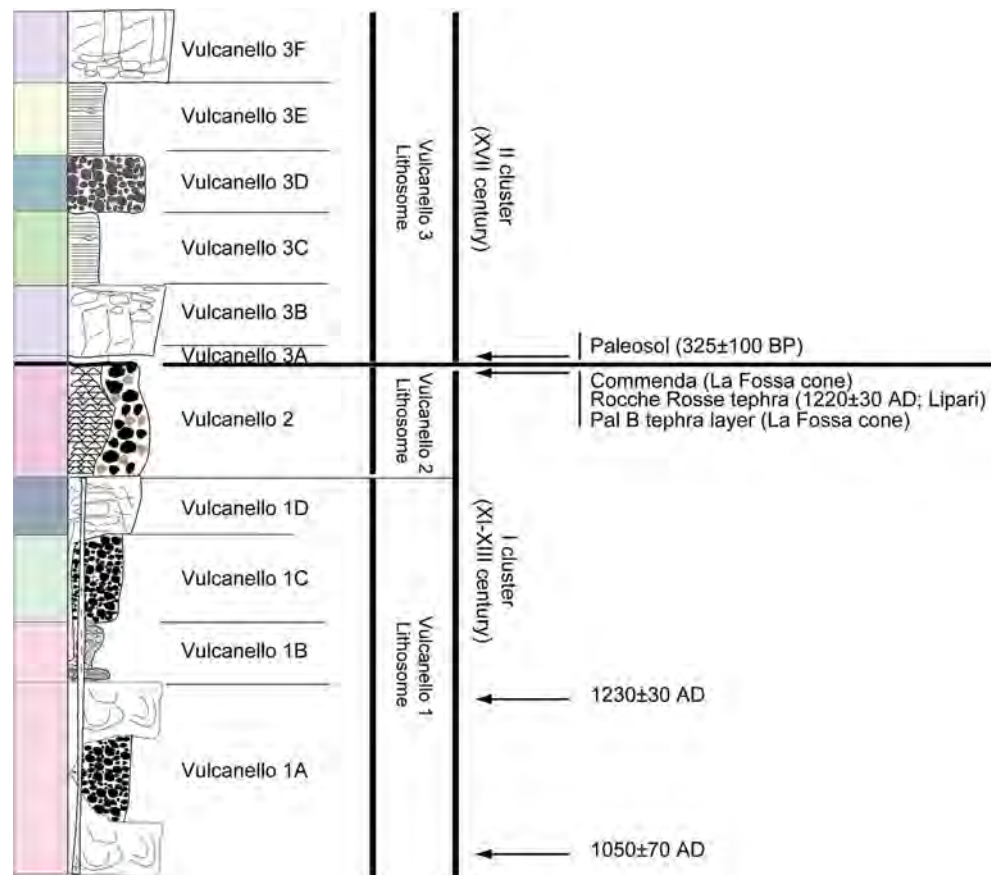
#### *Vulcanello 3 lithosome*

A paleosol dated at  $0.397 \pm 0.097$  ka (Keller 1980; De Astis et al. 2013) separates Vulcanello 2 from Vulcanello 3 lithosome which comprises six EUs (Table 3). The lower unit (Vulcanello 3A) corresponds to a fine-grained, gray to black

stratified ash deposit that opens the Vulcanello 3 activity (Fig. 9). This unit has been identified only in machine-made trenches and on the cliff on the northern sector, directly overlying the Rocche Rosse tephra from Lipari. Vulcanello 3A is overlain by the Vulcanello 3B lava (the Roveto lava described by Keller 1980; Fig. 9a) which was emitted from the north-western part of the cones and flowed in E–W direction. Being clearly exposed only within the crater walls and below the water tank located at the foot of the cone (outcrop 11 in Fig. 2a), the source area of Vulcanello 3B lava is unclear. The lava is overlain by a pyroclastic sequence which comprises three main tephra units (Vulcanello 3C, 3D, and 3E; Fig. 9b–d). Vulcanello 3C outcrops in the northwestern side (outcrops 11, 12, 13 in Fig. 2a) as a 3-m-thick, stratified, ash to lapilli deposit. It has been also found in some trenches on the lava platform (trenches 29, 30, 31 in Fig. 2). Vulcanello 3C is overlain by the Vulcanello 3D Unit, consisting of a 3-m-thick, massive to normally graded, grain-supported lapilli deposit (Fig. 9b; outcrop 14 in Fig. 2a). A fine ash-rich, thinly laminated, 3-m-thick deposit (Vulcanello 3E; Fig. 9) overlies Vulcanello 3D on the crater rim (outcrop 15 in Fig. 2a), on the cone flanks and in some trenches (29, 30, 31 Figs. 2a and 9). No juvenile clasts are clearly identifiable within this final deposit.

A final lava flow (Vulcanello 3F), which flowed in the same direction of Vulcanello 3B, closes the eruptive sequence of Vulcanello 3; although the Roveto lava flow (Vulcanello 3B, in our reconstruction) has been previously classified as a single unit (Davi et al. 2009; De Astis et al. 2013), we suggest that at least two different flows were emplaced. No clear geometric relationships exist on the cone, but the observations made along the sea cliff and the lack of the tephra sequence covering Vulcanello 3B lava flow on

**Fig. 3** Representative stratigraphic log of the whole Vulcanello eruptive activity (not to scale). Colors of the volcano-stratigraphic units as in Fig. 2



top of the final lava suggest the existence of two different lava flows.

### Morphological analysis and erupted volumes

The Vulcanello peninsula can be divided into two main geomorphological domains: the cone complex and the lava platform. The cone complex comprises three cones truncated by three craters. The transition from the crater rim to the cone flanks is marked by a change in slope from  $5^\circ$  to  $30^\circ$ . The cone flanks are dominated mainly by sheet erosion, while slope failures occur in the eastern sector. The Vulcanello cone complex is a constructional landform, as revealed by its high height ( $H$ )/base area ( $W_b$ ) ratio ( $H/W_b=0.76$ ); the summit area ( $W_s$ )/base area ratio ( $W_s/W_b=0.46$ ) indicates that it is slightly irregular in shape. The edifice has a conical form with an elliptical base, and the summit area is characterized by ESE–WSW striking major axes. The main destructive features are the three crater structures truncating the summit of the cone and the landslide scar that cuts the first cone in its eastern margin (Keller 1980; Romagnoli et al. 2013).

The lava platform consists of several lobes, which originate from the cone area (Fig. 2). The more evident lobe corresponds to the Valle dei Mostri lava that flowed in a

NNE direction from the boundary between the second and the third cone.

The volume of erupted products is defined by the volume of the Vulcanello peninsula (cones complex, lava platform, and Roveto + Valle dei Mostri lava flows) and the volume of the submarine lava field (Gamberi et al. 1997; Gamberi 2001; Romagnoli et al. 2013). The volumes (dense rock equivalent (DRE); Table 4) of the three cones vary between  $2 \times 10^{-3} \text{ km}^3$  for the first cone and  $3 \times 10^{-6} \text{ km}^3$  for the third cone, while the volumes of the three lavas vary between 0.345 (submarine lava field, considering  $3.5 \text{ km}^2$  and 70 m the area distribution and the average thickness) (Romagnoli et al. 2013) and  $3 \times 10^{-3} \text{ km}^3$  (Roveto + Valle dei Mostri lava flows). Vulcanello emplaced the maximum erupted volume during the Vulcanello 2 lithosome activity, with the emplacement of a very large submarine lava flow field. The erupted lava volume/total volume ratio varies between 0.93 (Vulcanello 1 lithosome) and 0.99 (Vulcanello 2 and 3 lithosomes), implying that the explosivity decreased in time, with the more explosive activity being related to Vulcanello 1. The average growth rate of the cone in the last 1000 years is therefore  $0.28 \text{ km}^3 \text{ kyear}^{-1}$ , lower than the value of  $0.96 \text{ km}^3 \text{ kyear}^{-1}$  estimated for the La Fossa cone (Di Traglia et al. 2013). It is worth noting that if only the cone volume is used as representative of the eruptive activity, this introduces

**Table 3** Main eruptive units of the Vulcanello lithosomes with related sedimentological features

Eruptive units	Bedding	Texture and grading	Clast size	Clast shape	Clast vesicularity	Welding	Lithic fragments
<b>Vulcanello 1 lithosome</b>							
Vulcanello 1A (lava)	Planar to lenticular; pahoehoe morphology	Massive	–	–	–	–	–
Vulcanello 1A (gray pyroclastics)	Planar	Massive	Fine to coarse lapilli; sporadic bombs	Irregular to elongated clasts	Moderate to high vesicularity	No welding	Lava
Vulcanello 1B	Planar	Massive (base), normally to reversely graded	Ash to lapilli; sporadic bombs	Irregular	High vesicularity	No welding	Lava
Vulcanello 1C	Stratified	Normally graded	Lapilli to bombs	Irregular	Moderate vesicularity	No welding	Lava; red scoriae
Vulcanello 1D	Planar	Massive	Bombs	Fluidal shape	Moderate vesicularity	Moderate to dense welding	No lithics
<b>Vulcanello 2 lithosome</b>							
Vulcanello 2	Planar, local lenticular	Massive (base), normal to reversely graded	Coarse ash to bombs	Highly elongated clasts	High vesicularity	No welding	Lava; red scoriae
<b>Vulcanello 3 lithosome</b>							
Vulcanello 3A	Stratified to thinly stratified	Massive	Fine ash	Irregular	–	No welding	–
Vulcanello 3B	Planar to lenticular; aa-lava morphology	Massive	–	–	–	–	–
Vulcanello 3C	Stratified to thinly stratified	Massive, impact structures	Fine ash, sporadic lapilli, and bombs	Irregular	–	No welding	Altered lava and scoriae
Vulcanello 3D	Planar, locally lenticular	Massive; normal graded	Coarse lapilli to bombs	Irregular	Moderate vesicularity	No welding	Altered lava and scoriae
Vulcanello 3E	Stratified to densely stratified	Massive, impact structures	Fine ash, sporadic lapilli, and bombs	Irregular	–	No welding	Altered lava and scoriae
Vulcanello 3F	Planar to lenticular; aa-lava morphology	Massive	–	–	–	–	–



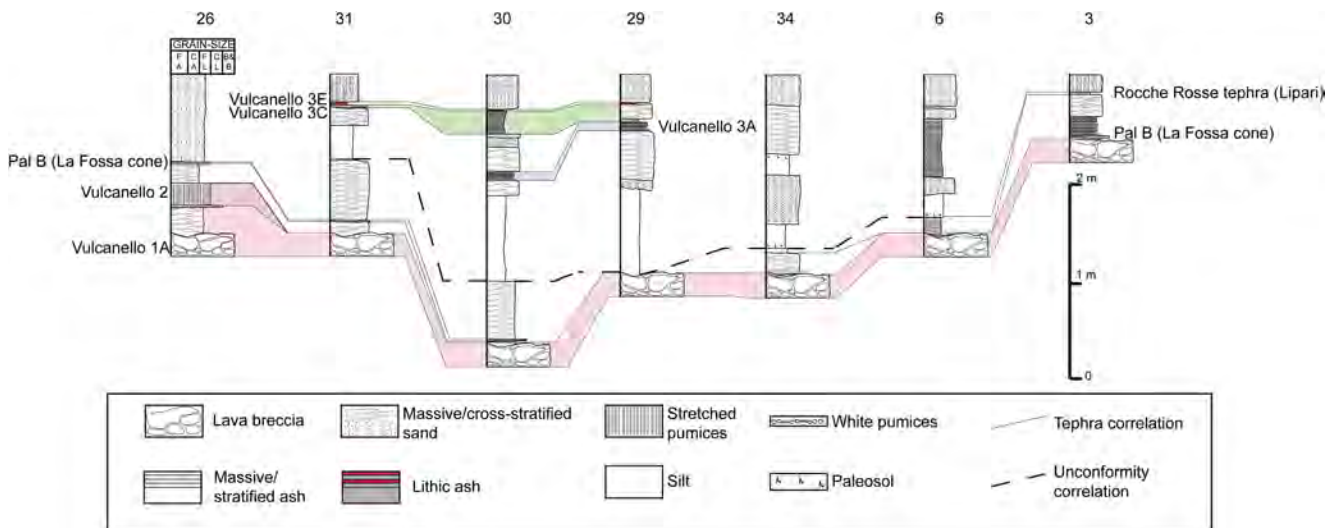


**Fig. 4** Stratigraphic relationships between Vulcanello, La Fossa, and Pilato (Lipari) deposits on the Vulcanello platform. Logs 26 and 3 are from natural sections while logs 31, 30, 29, 34, and 6 are from machine-

excavated and hand-dug pit trenches. The colors of the unit correlations refer to Fig. 2 and 3 unit colors

**Fig. 5** Outcrops of Vulcanello 1 lithosome. **a** Lava platform (Vulcanello 1A Eruptive Unit, facies plateau lava). **b** The two different facies in Vulcanello 1A Eruptive Unit, the plateau lava, and the gray pyroclastics; dike of Vulcanello 2 that cuts the entire stratigraphic sequence of Vulcanello 1 activity (outcrop n. 27 in Fig. 2). **c** Vulcanello 1 lithosome stratigraphic sequence (outcrop n. 26 in Fig. 2a)

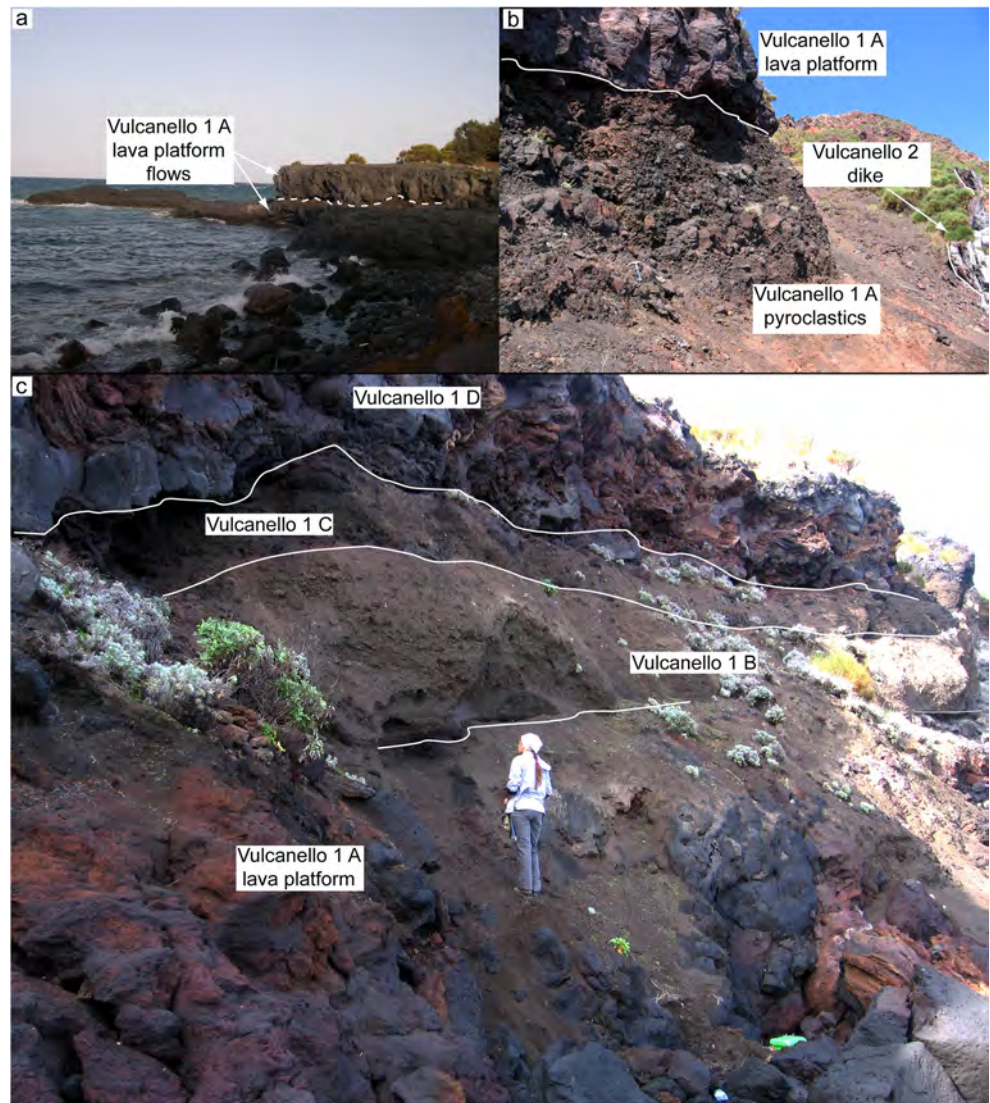
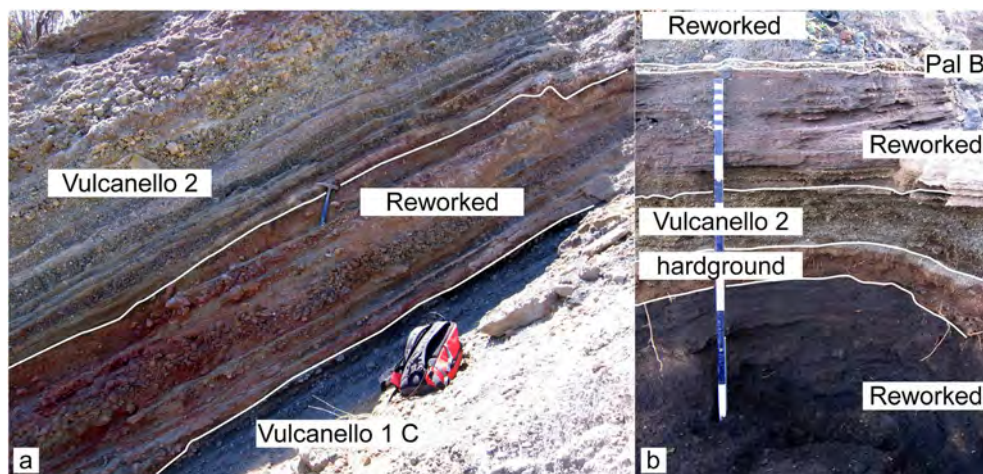


**Fig. 6** **a** Stratigraphic contact between Vulcanello 2 lithosome (Vulcanello 2 Eruptive Unit) and Vulcanello 1 lithosome (Vulcanello 1D Eruptive Unit) separated by reworked material on Vulcanello S–SE slope. **b** Stratigraphic relationship between Vulcanello 2 lithosome (Vulcanello 2 Eruptive Unit) and the Pal B rhyolitic layer from La Fossa activity on the northeast cliff of Vulcanello platform (outcrop n. 26 Fig. 2a)



an error between 5 and 20 % in the volume calculation (Di Traglia et al. 2009; Rodriguez-Gonzalez et al. 2010; Cimarelli et al. 2013).

### Petrography and whole-rock compositions

The samples of Vulcanello tephra selected for MI analyses have shoshonitic and latitic compositions when classified on a  $K_2O$  vs  $SiO_2$  wt% diagram and contain from 53 to 58 wt%  $SiO_2$  (Fig. 10; Table 5). The pillow lava of Vulcanello 2 has shoshonitic composition.

Geochemical and petrologic studies of Vulcanello rocks have mostly focused on lava samples (e.g., Davì et al. 2009, with 20 lava samples and three scoria and bomb samples; see also De Astis et al. 2013 and references therein). Our data on the pyroclastic products agree with the previous data in indicating shoshonitic composition for the Vulcanello 1 and Vulcanello 2 lithosomes and latitic composition for the Vulcanello 3 lithosome (Fig. 10). Davì et al. (2009) reported a shoshonitic composition for a bomb sampled at the base of Vulcanello 3 pyroclastic deposits. As regard the shoshonitic

rocks, the Vulcanello 2 tephra has lower  $MgO$  and  $Fe_2O_3$  and higher  $Al_2O_3$  and  $CaO$  with respect to Vulcanello 1A and B, suggesting higher olivine fractionation. The composition of the shoshonitic tephra samples is silica-undersaturated, with normative nepheline up to 10 %, while the latites are only slightly undersaturated (Table 5).

Overall, the primary mineral assemblage of tephra and lava products consists of clinopyroxene, plagioclase, olivine, and Fe–Ti oxides both in the shoshonitic and latitic products, with a relative decrease of olivine and the appearance of sanidine in the phenocryst assemblage of the latites. Leucite is also a common groundmass/microphenocryst phase in the shoshonites.

The lava units analyzed for the three different lithosomes (Vulcanello 1 plateau lava, Vulcanello 2 dike and submarine lava, and Vulcanello 3 lavas) display different petrographic characteristics.

The plateau lavas show clinopyroxene, olivine and plagioclase phenocrysts, and magnetite in a groundmass made of the same minerals, sanidine, and leucite. Clinopyroxene is predominant in phenocrysts and microphenocrysts.

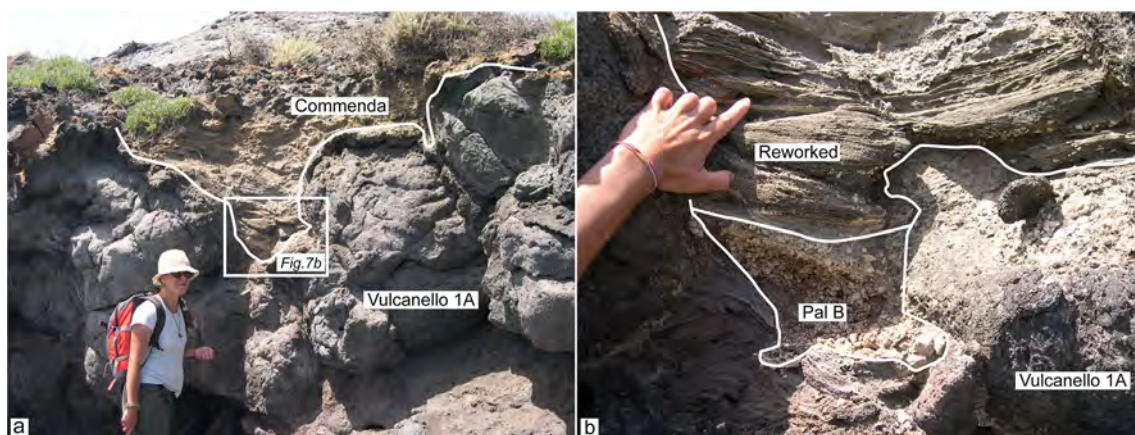


**Fig. 7** Stratigraphic relationships between Vulcanello 1 lithosome and Pal B rhyolitic layer from La Fossa activity on the southwest cliff of Vulcanello platform (outcrop n. 2 in Fig. 2a)

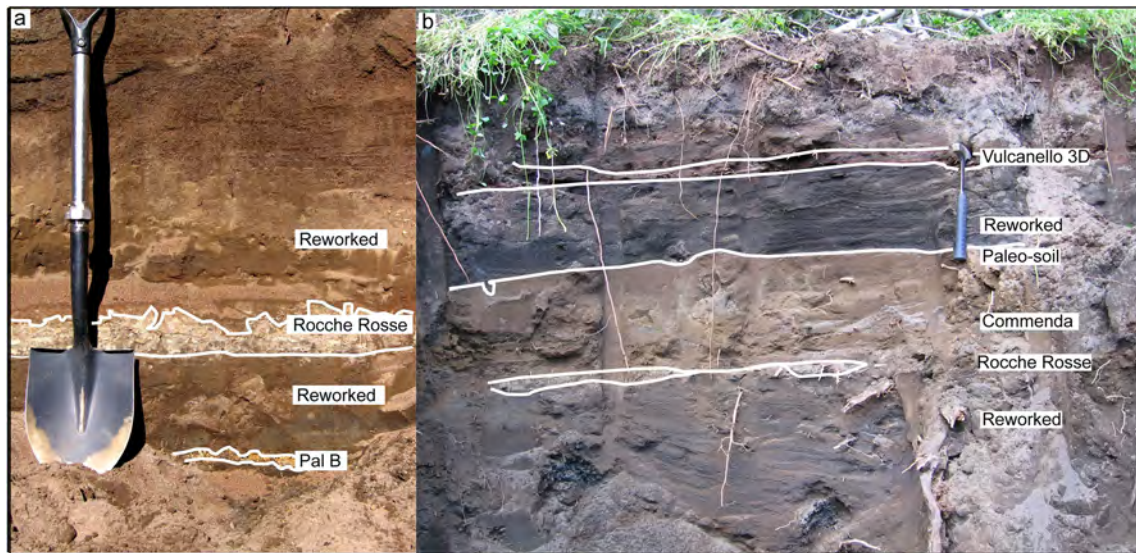


**Fig. 8** **a** Stratigraphic relationships between Pal B rhyolitic layer from La Fossa activity and Rocche Rosse tephra from the Mt. Pilato (Island of Lipari) activity on the Vulcanello platform (machine-excavated trench, site n. 31 Fig. 2a). **b** Stratigraphic relationships between the distal Rocche Rosse tephra from the Mt. Pilato and Commenda tephra from La Fossa

activity and the Vulcanello 3 lithosome (machine-excavated trench, site n. 29 Fig. 2). The paleosol marks the time interval between the first eruptive cluster, preceding the Commenda and the Rocche Rosse activity, and the second cluster, represented by the Vulcanello 3 activity

The dike is petrographically similar to the plateau lava, except for the lack of small-sized plagioclase and the acicular/skeletal shape of clinopyroxene microphenocrysts, suggestive of a rapid growth event before the final groundmass crystallization. The rounded shape of the large plagioclase crystals contrasts with the euhedrality of mafic minerals.

Similar textures of the phenocrysts and microphenocrysts are visible in the pillow lavas, differing only for the glassy groundmass: clinopyroxene was rapidly crystallizing immediately

before the eruption, while plagioclase lacks evidence of rapid crystallization and shows rounded corners. Opaques (magnetite) and apatite are accessories. The glassy brown groundmass shows sporadic clinopyroxene microlites.

The Vulcanello 3 lavas have phenocrysts of clinopyroxene, strongly zoned plagioclase with antirapakivi texture and minor sanidine, olivine, and opaques. Rounded xenocrysts of quartz and of minerals largely replaced by opaques are frequent. Rounded and sieve-textured plagioclase crystals

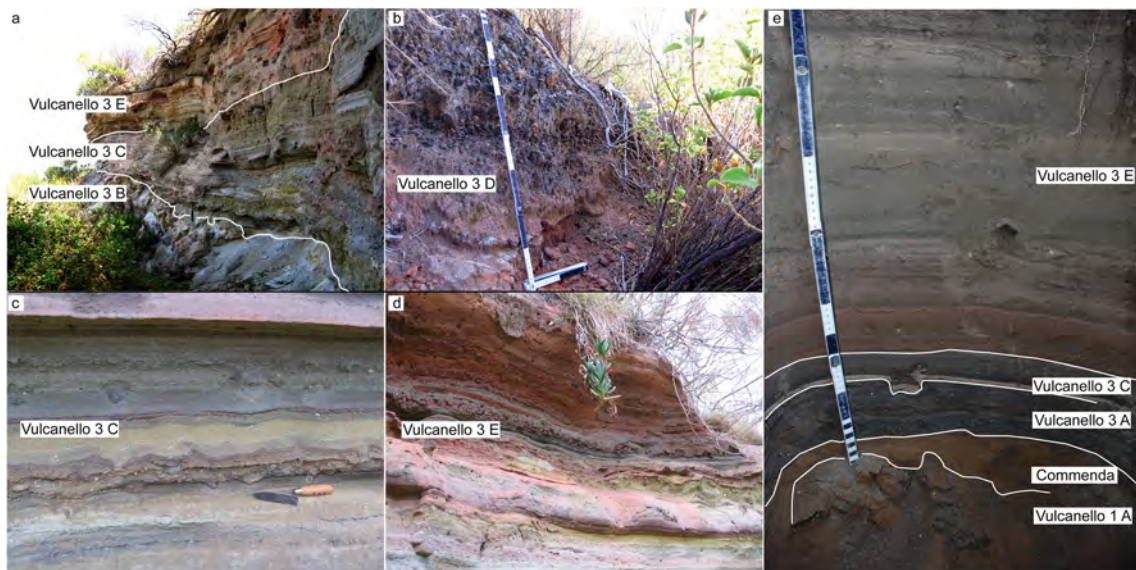


**Fig. 9** **a** Stratigraphic contacts between ashfall deposits (Vulcanello 3C and 3E Eruptive Units) from phreatic eruptions and lava flow deposit (Vulcanello 3B Eruptive Unit) of Vulcanello 3 lithosome (outcrop n. 11 in Fig. 2a). **b** Vulcanello 3 lithosome Vulcanello 3D Eruptive Unit. **c**, **d**

Details of the Vulcanello 3C and 3E Eruptive Units, respectively. **e** Tephra deposits on the Vulcanello platform (Vulcanello 1A) as found in hand-dug trench (site n. 34 in Fig. 2a), showing Vulcanello 3A, 3C, and 3E overlying the Commenda distal tephra

**Table 4** DEM-derived calculations of the Vulcanello lavas and tephra erupted volumes

	Volume (km <sup>3</sup> , DRE)
Vulcanello 3 cone	0.000025
Valle dei Mostri + Roveto lava flow	0.003
Vulcanello 2 cone	0.0015
Vulcanello 2 submarine lava field	0.245
Vulcanello 1 cone	0.002
Vulcanello 1 lava platform	0.026
	Lava volume/total volume
Vulcanello 3 lithosome	0.99
Vulcanello 2 lithosome	0.99
Vulcanello 1 lithosome	0.93

characterize the Roveto lava, similarly to the shoshonitic dike. The groundmass is dominated by feldspars. The Valle dei Mostri lava flow differs from the Roveto lava in the moderately higher phenocryst abundance and in the vesicular and partially oxidized groundmass.

## Melt inclusions

### Melt inclusion morphological features

Melt inclusion (MI) shape, relationship with the host-crystal, texture, and the presence of vapor bubbles and microlites were inspected as they unravel processes of inclusion formation and post-entrapment modification. Most of the MIs in Vulcanello olivine have spherical/subspherical shape and aphyric brown transparent glass (Fig. 11a–c), except those, finely crystallized, from the gray pyroclastics deposit of the Vulcanello

1A Unit. The 18 MIs analyzed have a size that ranges from 87  $\mu\text{m}$  (V3D5) to 605  $\mu\text{m}$  (V1C5) and are “fully enclosed” (Cervantes and Wallace 2003); that is, they can only communicate with the external melt by diffusion through the host crystal. None contains microlites.

Two MIs out of 18 have a “wrinkled” texture along the inclusion–host interface (Fig. 11a). The wrinkled texture is similar to that observed in MIs that have been experimentally reheated, as a result of a rapid dissolution of olivine. In the natural MIs, this textural feature may form due to magma mixing (Cervantes and Wallace 2003). The lack of shrinkage bubbles (Fig. 11; Roedder 1984) suggests that very little change in temperature occurred between the time the inclusions were originally trapped and the time of eruption, and that cooling during eruption was relatively rapid. Theoretical and experimental studies (Lowestern 1994; Tait 1992) confirm that rapid cooling allows MI to quench without bubble formation.

### Major element composition of melt inclusions and submarine glass samples

The measured major element composition of MI is reported in Table 6 together with the volatile content and the host crystal forsterite content, which was analyzed close to the MI. Details on data collection and number of analyses are reported in the Appendix.

The forsterite content of olivine phenocrysts ranges from Fo<sub>64,5</sub> to Fo<sub>70,2</sub> (Table 6). The low forsterite content is consistent with the low Mg# (Mg# = MgO/(MgO + FeO)) of the MI (Table 6), suggesting that their compositions were not strongly modified by post-entrapment crystallization of olivine along the inclusion walls. The correlation of the CaO/Al<sub>2</sub>O<sub>3</sub>

**Fig. 10** K<sub>2</sub>O vs SiO<sub>2</sub> wt% diagram (Peccerillo and Taylor 1976) of the Vulcanello samples studied in this work (bulk rock analysis, squares) compared with Vulcanello and La Fossa bulk rock composition (gray field) from Davi et al. (2009) and De Astis et al. (2013)

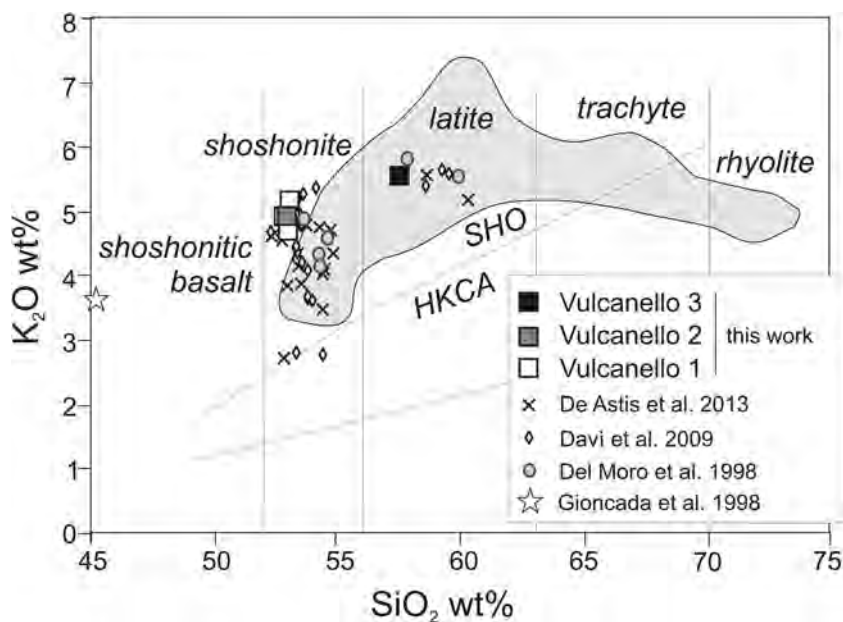


**Table 5** Whole-rock composition (XRF, wt%) and CIPW norm calculation of Vulcanello samples selected for the MI study

Unit Sample	Vulcanello 1A V1A	Vulcanello 1B V1B	Vulcanello 1C V1C	Vulcanello 2 V2	Vulcanello 3D V3D
SiO <sub>2</sub> (wt%)	51.79	52.54	52.54	52.61	57.23
TiO <sub>2</sub>	0.67	0.65	0.66	0.59	0.56
Al <sub>2</sub> O <sub>3</sub>	15.33	16.23	15.29	17.11	15.80
Fe <sub>2</sub> O <sub>3 T</sub>	8.74	8.38	8.71	7.29	7.12
MnO	0.14	0.15	0.15	0.13	0.14
MgO	4.18	4.03	4.59	3.31	3.07
CaO	8.14	7.67	8.56	9.11	5.72
Na <sub>2</sub> O	3.66	3.83	3.58	3.89	3.95
K <sub>2</sub> O	4.57	5.08	4.88	4.89	5.52
P <sub>2</sub> O <sub>5</sub>	0.45	0.45	0.43	0.41	0.38
L.O.I.	1.98	0.78	0.33	0.32	0.39
Sum	99.65	99.79	99.72	99.66	99.86
Alkali sum	8.23	8.91	8.46	8.78	9.47
Quartz	–	–	–	–	–
Albite	17.6	16.3	14.9	13.9	32.0
Anorthite	11.9	12.1	11.2	14.8	9.1
Orthoclase	27.0	30.0	28.8	28.9	32.6
Nepheline	7.2	8.7	8.3	10.3	0.7
Diopside	21.2	19.1	23.5	23.7	13.9
Olivine	8.3	8.5	8.2	4.6	7.4
Ilmenite	1.3	1.2	1.2	1.1	1.7
Magnetite	1.3	1.2	1.3	1.7	1.0
Apatite	1.0	1.0	1.0	0.9	0.9

All samples are juvenile lapilli

(incompatible elements in olivine) vs MgO ratio of the Vulcanello MIs (not shown) also suggests that the MIs have not been strongly affected by boundary layer enrichment processes (Métrich and Wallace 2008). To correct for any effects of post-entrapment crystallization, we added 0.1 % increments of equilibrium olivine, calculated using Fe–Mg partitioning (Roeder and Emslie 1970), to the composition of each inclusion until equilibrium with the host was achieved. The composition of each MI corrected for post-entrapment crystallization is reported in Table 6. All inclusions required less than 2 wt% of olivine addition to restore equilibrium, and some of them did not require any (Table 6). Therefore, the fractionation trend within V1C MI group reflects entrapment of melts with different evolution degree and not post-entrapment crystallization of the host.

The MIs have, after correction, SiO<sub>2</sub> contents that range from 51.5 wt% in V1C to 61.9 wt% in V3D (Table 6). The composition of the glass samples from Vulcanello 2 submarine lava nearly overlaps that of the MIs in olivine of Vulcanello 2 explosive activity (Table 7; Fig. 12).

In a K<sub>2</sub>O vs SiO<sub>2</sub> diagram (Fig. 12), the MI composition plots in the field of the Vulcanello and La Fossa products from Gioncada et al. (1998). When compared with the bulk rock analyses in variation diagrams (Fig. 12), the composition of

MI shows similar trends with initial increase of Al<sub>2</sub>O<sub>3</sub> and decrease of MgO, CaO, FeO, and TiO<sub>2</sub> and subsequent decrease of the same elements including Al<sub>2</sub>O<sub>3</sub>. These trends correspond to those already recognized in Vulcanello and La Fossa eruptive products (Del Moro et al. 1998; De Astis et al. 1997, 2013). The major element composition of the MI, therefore, indicates that they are representative of the compositions of the different magma batches that fed the activity of Vulcanello during its entire history.

#### *Volatiles in melt inclusions and pressure of entrapment*

The H<sub>2</sub>O concentrations in MI from Vulcanello's explosive activity, corrected for post-entrapment olivine crystallization, are ≤1 wt%, with average values ( $\pm 1\sigma$ ) of  $0.68 \pm 0.31$  wt% for Vulcanello 1,  $0.57 \pm 0.23$  wt% for Vulcanello 2, and  $0.56 \pm 0.35$  wt% for Vulcanello 3 (Table 6; Fig. 12). The highest H<sub>2</sub>O concentrations are recorded in Vulcanello 1 (V1C) with values up to 1.32 wt%, matching with the highest concentration of sulfur (Fig. 12). The chlorine dissolved in MI increases with the magmatic evolution, while the sulfur content decreases (Fig. 12). Fluorine concentration, on the contrary, is constant (Fig. 12). The H<sub>2</sub>O dissolved in submarine glass samples is, on average, lower (0.36 wt%) than that in MI.

Using the H<sub>2</sub>O concentration, it is possible to estimate vapor saturation pressures and therefore the minimum pressure of entrapment or last equilibration (Anderson et al. 1989). All the analyzed MIs were fully enclosed without vapor bubble, therefore suitable for entrapment pressure estimates (Cervantes and Wallace 2003). The saturation pressure was assessed on the basis of the empirical H<sub>2</sub>O solubility model of Moore et al. (1998), using the corrected MI composition and a temperature of 1100 °C from microthermometric results (Gioncada et al. 1998). The values obtained range from 0.2 MPa to a maximum of 21.2 MPa (Table 6). On the basis of a geobaric gradient of 27.5 MPa/km for a continental crust average density of 2.8 g/cm<sup>3</sup>, the minimum depth of entrapment/last equilibration is lower than 1 km beneath the volcano.

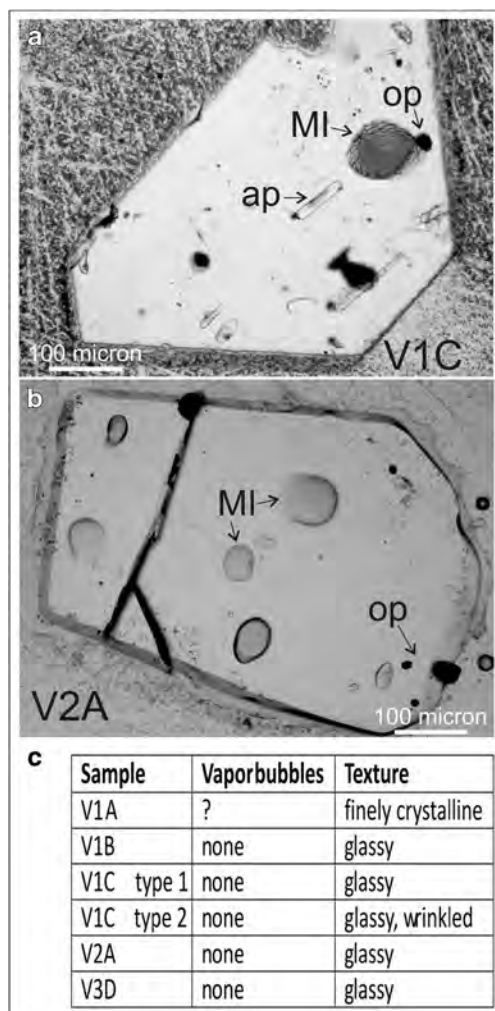


**Fig. 11** Microphotographs of melt inclusions in olivine after sectioning for infrared spectroscopy. **a** Wrinkled texture in fully enclosed melt inclusion in Vulcanello 1C Eruptive Unit. **b** Glassy texture in fully enclosed melt inclusions in Vulcanello 2 Eruptive Unit. **c** Main morphological features of MI in the selected samples (presence of vapor bubbles, texture)

## Discussion

### Reconstruction of the eruptive activity

The data reported support our interpretation that the activity forming the early subaerial part of Vulcanello (Vulcanello 1 lithosome) started in the eleventh to twelfth centuries AD as proposed by Arrighi et al. (2006), with emplacement of the lava platform (Vulcanello 1A plateau lava) which comprises several superimposed lava flows with a total volume of  $2.6 \times 10^{-2}$  km<sup>3</sup>. The effusive activity was coeval with explosive activity (Vulcanello 1A gray pyroclastics, 1B, 1C, 1D) which formed a cinder cone with a volume of  $2 \times 10^{-3}$  km<sup>3</sup>. We infer that emergence of the Vulcanello islet represented the final stage of growth through the accumulation of pillow lavas erupted in submarine environments and presently recognized along the northeastern submarine slopes of the islet (Gamberi and Marani 1997; Romagnoli et al. 2013) and accompanied by explosive activity at the surface, as reported in historical accounts (Mercalli and Silvestri 1891; De Fiore 1922).

After a short time break marked by deposition of intercalated epiclastic deposits within the tephra sequence, the activity resumed with explosive eruptions (Vulcanello 2) which led to the formation of a second cone (total volume of  $1.5 \times 10^{-4}$  km<sup>3</sup>). The recognition of the rhyolitic pumice from La Fossa cone (Pal B; Fig. 4) and of the Rocche Rosse tephra from Lipari on top of the Vulcanello 2 lithosome (Di Traglia et al. 2013) suggests that the beginning of the Vulcanello activity was close in time to the reactivation of the La Fossa cone in the late Middle Ages (~AD 1200).

About five centuries of rest followed, before activity of Vulcanello resumed with the emplacement of a latitic lava flow (Vulcanello 3B, Roveto lava flow) with a total volume of  $3 \times 10^{-3}$  km<sup>3</sup>, heralded by an initial phase of explosive activity (Vulcanello 3A). In some previous reconstructions (Davi et al. 2009), Vulcanello 3B is attributed to the final stage of Vulcanello 2 activity, but based on its relationship with the ash found below the lava, we consider Vulcanello 3B as part of the Vulcanello 3 cycle. The lava emission was followed by three explosive phases (Vulcanello 3C, 3D, and 3E) that led the edification of the third cone with a volume of  $2.5 \times 10^{-3}$  km<sup>3</sup>. The first of these events (Vulcanello 3C) had a strong phreatic signature, with no or little magma involvement. The emission of strongly altered lithic material after the emplacement of the Roveto lava flow, coupled to the intense alteration affecting the Roveto lava outcrops close to the crater area, suggests that, in a relatively short period of rest, the intense magmatic degassing of the shallow magma batch induced hydrothermal circulation and consequent alteration in the area of the Vulcanello 3 crater. The Vulcanello 3C phreatic phase was followed by the Vulcanello 3D explosive activity, having a clear magmatic origin. Instead, the following explosive phase (Vulcanello 3E) which formed the upper part of the

**Table 6** Major element and volatile compositions measured on melt inclusions (above) and recalculated compositions (below, see text for recalculations details)

Sample Inclusion	V1B 1	V1B 3	V1B 4	V1B 5	V1B 6	V1C 1	V1C 4	V1C 5	V2 1d	V2 4d	V2 1p	V2 2p	V2 4p	V3D 1	V3D 2	V3D 3	V3D 4	V3D 5	
SiO <sub>2</sub> wt%	53.35	54.94	53.75	55.44	55.87	52.10	52.61	51.12	53.29	55.48	54.73	56.77	54.66	61.66	59.50	59.95	59.89	56.33	
TiO <sub>2</sub>	0.64	0.58	0.65	0.58	0.71	0.66	0.63	0.64	0.60	0.60	0.60	0.58	0.59	0.58	0.57	0.60	0.40	0.61	
Al <sub>2</sub> O <sub>3</sub>	18.16	17.84	17.77	17.74	17.16	17.12	18.02	16.34	17.33	18.24	18.36	16.87	17.83	17.24	17.23	17.17	17.35	19.07	
FeO <sub>T</sub>	7.37	6.69	7.46	6.81	6.62	8.49	7.77	9.32	6.65	6.84	6.92	6.47	6.70	5.08	5.23	5.18	5.06	4.91	
MnO	0.16	0.15	0.15	0.15	0.16	0.17	0.15	0.19	0.15	0.16	0.15	0.14	0.15	0.12	0.11	0.12	0.11	0.10	
MgO	2.17	1.92	2.22	1.71	1.80	2.91	2.82	4.26	1.83	1.83	1.74	1.79	1.99	0.96	1.09	1.10	1.13	1.22	
CaO	4.91	4.00	5.12	3.62	3.77	6.52	6.05	5.55	3.66	3.88	3.85	3.79	4.09	2.49	3.05	2.77	2.96	3.66	
Na <sub>2</sub> O	4.79	5.23	4.74	5.14	4.96	4.15	4.57	4.25	5.00	4.71	4.66	5.18	4.52	4.74	5.43	5.35	4.42	4.65	
K <sub>2</sub> O	6.71	7.09	6.63	7.11	7.00	5.77	6.10	5.70	7.09	7.09	7.25	7.18	7.02	5.13	7.20	6.21	7.37	7.30	
P <sub>2</sub> O <sub>5</sub>	0.60	0.59	0.57	0.55	0.78	0.81	0.56	0.81	0.63	0.60	0.59	0.57	0.59	0.30	0.43	0.29	0.59	0.36	
S	0.03	0.01	0.04	0.02	0.02	0.03	0.05	0.04	0.01	0.02	0.02	0.02	0.02	0.01	0.02	0.02	0.02	0.03	
Cl	0.31	0.29	0.32	0.33	0.33	0.31	0.30	0.31	0.27	0.31	0.32	0.29	0.29	0.37	0.37	0.41	0.31	0.31	
F	0.12	0.16	0.14	0.12	0.13	0.14	0.13	0.13	0.14	0.18	0.14	0.19	0.16	0.12	0.15	0.12	0.12	0.14	
H <sub>2</sub> O	0.69	0.09	0.65	0.57	0.60	0.88	1.32	0.64	0.69	0.36	0.49	0.35	0.88	0.12	0.38	0.95	0.83	0.42	
Total	100.02	99.59	100.22	99.87	99.86	100.05	101.07	99.28	97.33	100.3	99.90	100.18	99.49	98.92	100.4	100.24	100.55	99.11	
Fo host	67.97	68.27	68.81	68.25	67.73	70.14	68.28	68.43	69.5	68.91	68.51	70.23	68.34	65.14	64.73	64.53	64.45	69.39	
Mg#	0.39	0.39	0.4	0.36	0.37	0.41	0.45	0.51	0.38	0.37	0.36	0.38	0.39	0.29	0.32	0.32	0.33	0.33	
Composition corrected for post-entrapment crystallization:																			
%Ol added	0.0	0.1	0.0	1.2	0.3	0.0	0.0	0.0	0.9	0.9	1.3	1.1	0.0	1.6	1.0	0.8	0.5	1.2	
SiO <sub>2</sub> wt%	53.33	55.15	53.63	55.29	55.88	52.07	52.05	51.50	54.59	55.16	54.54	56.44	54.93	61.91	58.82	59.6	59.43	56.6	
TiO <sub>2</sub>	0.64	0.58	0.65	0.58	0.7	0.66	0.63	0.64	0.61	0.59	0.65	0.57	0.6	0.58	0.56	0.6	0.4	0.61	
Al <sub>2</sub> O <sub>3</sub>	18.16	17.90	17.73	17.54	17.13	17.11	17.83	16.46	17.64	18.03	18.14	16.66	17.92	17.15	16.93	16.98	17.16	19.00	
FeO <sub>T</sub>	7.37	6.74	7.45	7.09	6.7	8.48	7.66	9.39	7.03	7.01	7.21	6.69	6.7	5.59	5.46	5.38	5.17	5.25	
MnO	0.16	0.15	0.15	0.15	0.16	0.18	0.15	0.19	0.15	0.16	0.15	0.14	0.15	0.12	0.11	0.12	0.11	0.1	
MgO	2.17	1.96	2.21	2.08	1.89	2.91	2.79	4.29	2.17	2.11	2.15	2.15	1.998	1.44	1.38	1.34	1.27	1.62	
CaO	4.91	4.01	5.11	3.58	3.76	6.51	5.98	5.59	3.71	3.83	3.8	3.74	4.11	2.48	3.00	2.74	2.92	3.64	
Na <sub>2</sub> O	4.79	5.24	4.73	5.08	4.95	4.15	4.52	4.28	5.08	4.66	4.6	5.11	4.54	4.71	5.34	5.29	4.38	4.63	
K <sub>2</sub> O	6.70	7.12	6.62	7.03	6.98	5.76	6.03	5.74	7.21	7.01	7.17	7.09	7.05	5.105	7.07	6.14	7.29	7.28	
P <sub>2</sub> O <sub>5</sub>	0.60	0.59	0.57	0.54	0.75	0.82	0.56	0.81	0.65	0.59	0.59	0.56	0.6	0.30	0.43	0.29	0.58	0.36	
S	0.04	0.02	0.04	0.02	0.02	0.03	0.05	0.04	0.01	0.02	0.02	0.02	0.02	0.01	0.02	0.02	0.02	0.03	
Cl	0.32	0.3	0.32	0.33	0.33	0.31	0.3	0.31	0.28	0.31	0.32	0.29	0.29	0.37	0.36	0.41	0.30	0.31	
F	0.13	0.17	0.14	0.12	0.13	0.14	0.13	0.14	0.15	0.18	0.14	0.19	0.16	0.12	0.15	0.12	0.12	0.14	
H <sub>2</sub> O	0.69	0.09	0.65	0.58	0.62	0.88	1.32	0.63	0.72	0.36	0.5	0.36	0.89	0.12	0.39	0.98	0.85	0.43	
Total	100.00	100.00	100.00	100.00	100.00	100.00	100.00	100.00	100.00	100.00	100.00	100.00	100.00	100.00	100.00	100.00	100.00	100.00	

Table 6 (continued)

Sample Inclusion	V1B 1	V1B 3	V1B 4	V1B 5	V1B 6	V1C 1	V1C 4	V1C 5	V2 1d	V2 4d	V2 1p	V2 2p	V2 4p	V3D 1	V3D 2	V3D 3	V3D 4	V3D 5	
Mg#	0.39	0.39	0.39	0.38	0.40	0.40	0.45	0.51	0.41	0.40	0.40	0.41	0.40	0.36	0.35	0.35	0.35	0.35	0.40
P (MPa)	7.3	0.2	6.4	5.2	5.9	10.6	21.2	6.0	7.6	2.4	4.1	2.3	11.0	0.4	2.7	12.5	10.0	3.2	

Data in wt%. Each major element analysis is the mean of several analyses on the same MI (see "Methods" section in Supplementary material). Total iron as FeO<sub>T</sub>. Mg# is  $\text{Mg}^{2+}/(\text{Mg}^{2+} + \text{Fe}^{2+})$ , assuming that 80 % of the total iron is present as Fe<sup>2+</sup>. P is the vapor saturation pressure in Pascal calculated following Moore et al. (1998)

cone was again dominated by altered material giving a definite reddish color to the ash deposits. The activity of Vulcanello 3 was closed by the emplacement of a final lava (Vulcanello 3F) which mostly flowed in the same direction of the Roveto lava. The presence of a second cluster of eruptions was also confirmed by historical accounts, which described frequent eruptive activity at Vulcanello, La Fossa cone, and Forgia craters during the seventeenth to eighteenth centuries (Mercalli and Silvestri 1891; De Fiore 1922). Moreover, the deposits related to the activity of Vulcanello 3 are coeval with the lower part of the GCEC (Di Traglia et al. 2013). On the basis of historical chronicles and stratigraphic reconstructions, we can thus infer that during this period, multiple vents were active at the Island of Vulcano. The behavior of Vulcanello resembles that of La Fossa cone, with several eruptions not equally spaced but mostly clustered in time. Clusters of eruptions have been identified at several mafic-to-intermediate central volcanoes, such as Cotopaxi (Pistolesi et al. 2011), Vesuvius (Arrighi et al. 2001; Principe et al. 2004), Etna (Branca and Del Carlo 2005; Allard et al. 2006), and at mafic volcanic fields (Garrotxa Volcanic Field; Cimarelli et al. 2013), and are related to the interplay between tectonic stress and variable magma supply from depth (Takada 1999).

The overall Vulcanello eruption rate (i.e., the eruption rate during the entire cycle of the volcano) is estimated at  $0.28 \text{ km}^3 \text{ kyear}^{-1}$ ; if considering only the Vulcanello 1 and 2 lithosomes, the average eruption rate rises to  $1.37 \text{ km}^3 \text{ kyear}^{-1}$ . For comparison, the eruption rate of the nearby La Fossa cone is within this range ( $0.96 \text{ km}^3 \text{ kyear}^{-1}$ ; Di Traglia et al. 2013), implying that Vulcanello was fed by short-lived magma batches ( $10^2$ – $10^3$  years), as also proposed by Hobden et al. (2002) for the Ngauruhoe volcano (New Zealand), which is characterized by a comparable growth rate ( $0.9 \text{ km}^3 \text{ kyear}^{-1}$ ).

### Geochemical and petrological constraints for the Vulcanello shallow storage system

The magmas erupted at Vulcanello register an appreciable, although modest, differentiation range (Davi et al. 2009; De Astis et al. 2013; this work). The least differentiated magmas were the shoshonites erupted in Vulcanello1 phase, fed by a slightly zoned magma batch, with the most evolved magmas erupted first. The magmas of Vulcanello 2 phase were only slightly more evolved than those of Vulcanello 1, while during Vulcanello 3 phase the erupted magmas were definitely the most differentiated at Vulcanello.

The comparison of the chemical composition of the MIs from Vulcanello explosive activity with the bulk rock data available on lavas and tephra indicates that MI can be confidently considered representative of the different magma batches that fed the volcanic activity of Vulcanello (Fig. 12). Therefore, the MIs record the entire differentiation history of Vulcanello magmas.



**Table 7** Major element compositions and volatile content of glass of the submarine lava from Vulcanello 2 activity

Sample Fragment	V2p V2p2	V2p V2p3	V2p V2p4	V2p V2p5
SiO <sub>2</sub> wt%	54.76	54.86	56.41	56.37
TiO <sub>2</sub>	0.63	0.63	0.66	0.66
Al <sub>2</sub> O <sub>3</sub>	17.37	17.58	17.88	17.68
FeO <sub>T</sub>	6.59	6.66	7.00	6.66
MnO	0.13	0.14	0.15	0.16
MgO	1.84	1.84	1.93	1.94
CaO	4.18	4.19	4.37	4.35
Na <sub>2</sub> O	4.96	4.85	3.8	4.6
K <sub>2</sub> O	6.99	6.97	5.47	6.46
P <sub>2</sub> O <sub>5</sub>	0.61	0.6	0.65	0.63
S	0.02	0.02	0.02	0.02
Cl	0.31	0.31	0.33	0.33
F	0.17	0.11	0.14	0.11
Total	98.56	98.76	98.82	99.97
H <sub>2</sub> O	0.43	0.26	0.34	0.42
Mg#	0.33	0.33	0.33	0.34
P (MPa)	3.2	1.4	2.1	3.0

Each major element analysis is the mean of several analyses on the same fragment. Total iron is reported as FeO<sub>T</sub>. All analyses are in wt%. Mg# and P are defined as in Table 5

The largely spherical shapes of the MIs in all the studied samples, together with the euhedral shape of the olivine host crystals, suggest low cooling rates on the order of 1 to 2 °C/h (Métrich and Wallace 2008) and rule out the growth of olivine under strong undercooling conditions during rapid magma ascent. The crystallization, therefore, occurred during the pre-eruptive storage of each magma batch, having progressively more evolved composition.

The volatile content of Vulcanello MIs can be used to assess the degassing history and the last magma storage depth. On the basis of MI textural features, it can be inferred that their low content of H<sub>2</sub>O (0.36–1.32 wt%) and their sulfur, chlorine, and fluorine content (100–500, 2800–4100, 1200–1900 ppm, respectively) are representative of the pre-eruptive volatile budget. The CO<sub>2</sub> content is below the detection limit (50 ppm). Due to its low solubility, CO<sub>2</sub> tends to degas almost entirely before significant H<sub>2</sub>O is lost. The lack of measurable CO<sub>2</sub> in Vulcanello MIs is in agreement with previous data, indicating that CO<sub>2</sub> is exsolved deep below Vulcano (Gioncada et al. 1998).

Loss of H<sub>2</sub>O from MI due to hydrogen diffusion through the host commonly occurs during magma ascent, in order to reach equilibrium with the outer melt (Watson 1994; Chen et al. 2011, 2013; Bucholz et al. 2013; Lloyd et al. 2013). However, on the basis of the comparison of the radius of Vulcanello MI (~70 μm) and the olivine size (0.7–0.5 mm) with the results of Chen et al. (2013) and the fact that MIs were

selected far from the host rim, it is unlikely that water loss by hydrogen diffusion affected significantly the studied MI. Therefore, the measured volatile content is likely to be representative of the saturation pressure of a magma batch equilibrated at about 1 km beneath the volcano.

Previous works (Zanon et al. 2003; Peccerillo et al. 2006) identified for the Vulcanello feeding system a 20 km-deep mafic magma storage level, close to the Moho, and a shallower reservoir located at 3–5 km, related to a lithological boundary between the metamorphic basement and the base of the volcanic complex. An additional magma reservoir at 1.3 km was identified below La Fossa (Clocchiatti et al. 1994a).

The MI textural and analytical data obtained in this work indicate for Vulcanello a period of magma residence at about 1 km of depth, suggesting a similarity of the plumbing system with La Fossa cone. Although all the analyzed MIs were trapped at shallow depths, the Vulcanello 1 shoshonites may still signal the ascent of magma from deeper storage (Vetere et al. 2007; Davì et al. 2009).

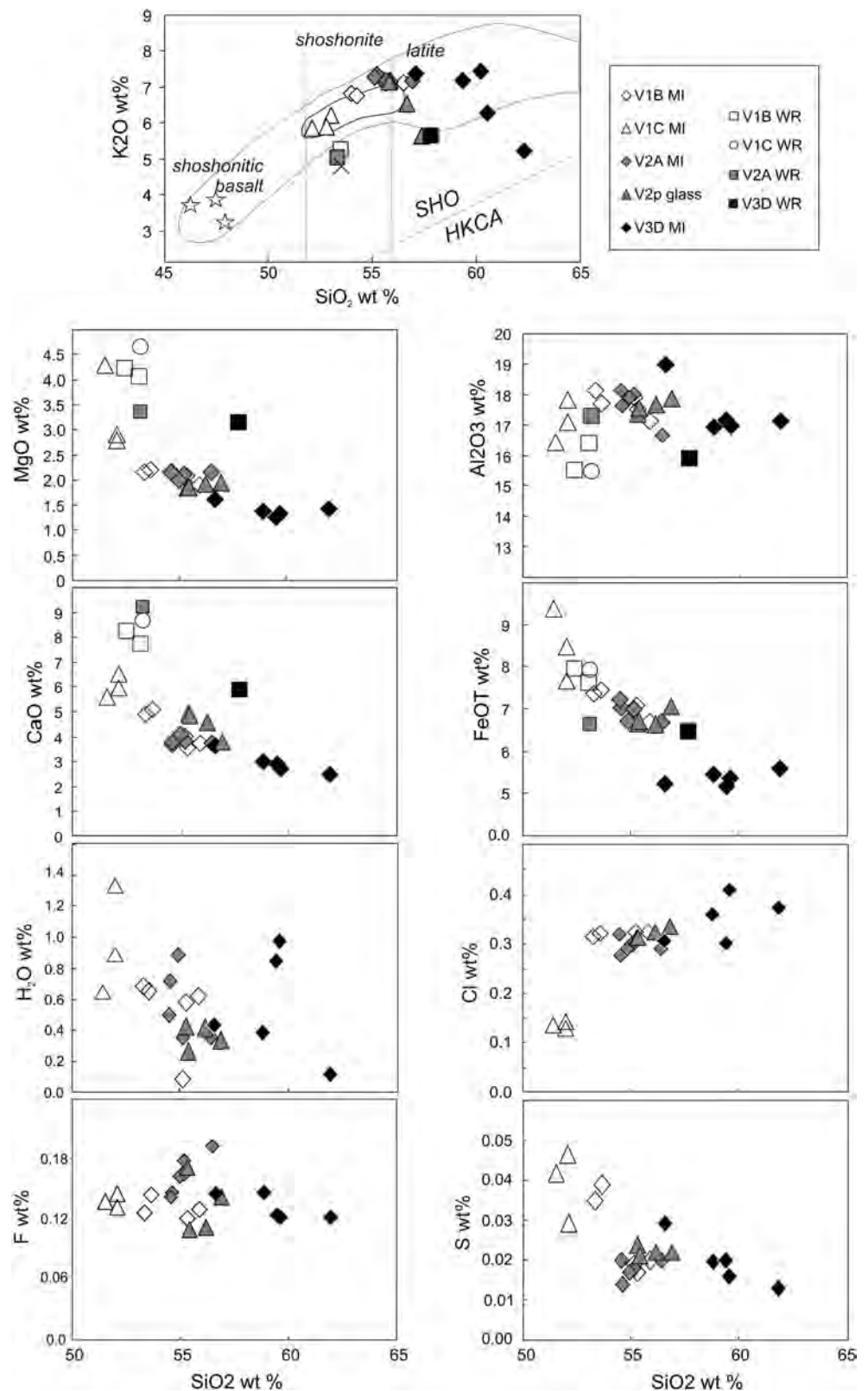
The latter cluster of Vulcanello eruptive episodes occurred after magma differentiation to latite and concomitant with development of shallow hydrothermal alteration. Passive degassing at Vulcanello, as well as at La Fossa cone (Fulignati et al. 1998; Carapezza et al. 2011), can be the result of magma storage and evolution in a shallow reservoir fed by a deeper system (Clocchiatti et al. 1994b). During the differentiation of shoshonite to latite, sulfur and water were lost through open-system degassing at shallow depth. Chlorine, in contrast, increased during differentiation from about 52 to 55–56 wt% SiO<sub>2</sub>, indicating incompatible behavior consistent with the low partitioning of chlorine in the aqueous fluid phase at low pressure. This behavior mimics that observed at La Fossa (Clocchiatti et al. 1994b), confirming the similarities between these two volcanoes.

### Vulcanello feeding system

Zanon et al. (2003) report that the Vulcanello activity provides evidence of the deepest (about 20 km) storage zone of the polybaric plumbing system that fed the island of Vulcano (Fig. 13). A shallower shoshonitic storage system located at depths of 3–5 km (Zanon et al. 2003; De Ritis et al. 2013) was then identified as the source of the primitive magmas which fed both Vulcanello and La Fossa cone activity (Gioncada et al. 1998). Seismic data also suggests the existence of a seismogenic structure below Vulcanello, interpreted as a discontinuity linking the deep (21 km) reservoir to the magma accumulation zones at 3–5 km and representing the preferential pathway along which magma may move from the deep system to the intermediate storage zone (Gambino et al. 2012).

The Vulcanello transport system is probably tied to the northern ring fault of the La Fossa caldera (Ventura et al.

**Fig. 12** Major element variation diagrams for Vulcanello melt inclusions (MIs), glass of the pillow lavas (V2p glass), and whole-rock (WR) samples. In the  $K_2O$  vs  $SiO_2$  plot, fields for MI composition of the Fossa products (*dotted line*) and for Vulcanello 1 products (*full line*) after Gioncada et al. (1998) are reported. The stars indicate the parent basaltic composition of the Vulcanello magmas (Davi et al. 2009) found in MI in Fo90 olivine (Gioncada et al. 1998). For comparison to the whole rocks, the MI composition is plotted after normalization of major elements to 100



1999; Davi et al. 2009). We hypothesize that magma batches repeatedly intruded the ring fault structure, supplying the activity of the three Vulcanello lithosomes. Intrusion of magma

along a ring fault depends on two driving mechanisms (Rubin 1995): (i) the overcoming of the minimum principal stress ( $\sigma_3$ ) by magmatic pressure (main driving force until

reaching the level of neutral buoyancy) (Takada 1999) and (ii) the magma overpressure component (crucial for the lateral expansion of dikes) (Rubin 1995). Moreover, ring faults help sheet intrusions to reach the surface, providing an almost homogeneous (in terms of stress field homogenization) pathway for reaching the surface (Browning and Gudmundsson 2014). If we consider that the magma ascent is only due to buoyancy, the magmatic overpressure component  $p_e$  may be estimated using the following relation (Vetere et al. 2007):

$$p_m = \Delta\rho gh \quad (1)$$

where  $\Delta\rho$  is the difference between the density of the country rock and the melt (average  $335 \text{ kg/m}^3$ ; Vetere et al. 2007),  $g$  is the gravity, and  $h$  is the vertical length of the dike (3–5-km depth).

The obtained values are in the order of 10–16 MPa, within the range of magma overpressure in basaltic dikes (Becerril et al. 2013). For a volcano such as the La Fossa caldera, both the sheet dip and the geometry of the shallow magma chamber make the length of the sheet,  $L$ , greater than the depth of the magma chamber  $z$  (Gudmundsson 2011):

$$L = z / \sin\alpha \quad (2)$$

where  $\alpha$  is the dip of the sheet ( $43^\circ$  for the Vulcanello 2 feeder dike). The length of the sheet  $L$  ranges between 4 and 7 km, and given its geometry, sheet  $L$  could be defined as cone sheet ( $30$ – $45^\circ$ , inwardly dipping sheet intrusion; Walter and Troll 2001). Considering elongation of the Vulcanello 1 cone (500–700 m) as a proxy for the length ( $d$ ) of the feeder sheet (the intersection between the sheet and the surface), we can evaluate the depth ( $h$ ) of the magma chamber (Becerril et al. 2013):

$$h = \frac{\Delta u E}{2d \Delta\rho(1-\nu^2)} - \frac{\rho m - \sigma_d}{g \Delta\rho} \quad (3)$$

where  $E$  and  $\nu$  are the host rock Young's modulus and Poisson's ratio, respectively, and  $\sigma_d$  is the differential stress (the difference between the vertical stress and the minimum principal horizontal stress). The obtained value for the magma chamber depth is in the range 4–6 km, which agrees with previous estimates based on petrological data (Zanon et al. 2003).

The Vulcanello 2 feeder dike is NE–SW-oriented, in agreement with the direction of the La Fossa caldera ring fault (Romagnoli et al. 2013), while the submarine lava field is aligned with the Vulcanello cones in a ENE–WSW direction. This implies that buoyant upward flow of the magma that fed the explosive activity rose along a cone sheet while the outward flow rose toward the ENE buttressed from the conduit, as it has been observed in other scoria cones (Petronis et al. 2013) and central volcanoes (Intrieri et al. 2013). Horizontally

propagating intrusions can only be emplaced if the edifice load prevents eruption through the central area and if magma is negatively buoyant at shallow depth (Pinel and Jaupart 2004). In regard to the activity of Vulcanello 3 lithosome, we hypothesize that the shoshonitic magma evolved to latite through fractionation and crustal assimilation at shallow depth. Evidence of the very shallow magma storage and differentiation in the Vulcanello 3 activity is testified by the occurrence of altered materials ejected during phreatic activity and by an extensive fumarole field associated with the weathered zone in the northern side of the Vulcanello cones.

Vetere et al. (2007) calculated a magma rise speed in the range 0.089 to 0.45 m/s for the Vulcanello eruptive system. This rise speed range falls within that of Strombolian to Hawaiian activity (Parfitt 2004) and is consistent with the negligible water loss for hydrogen diffusion (Chen et al. 2013; Le Voyer et al. 2014). Considering the length of the feeding sheet and the rise speed, we infer an ascent time in the range 2–22 h, in good agreement with the mixed effusive–explosive eruptive style (Scandone et al. 2007).

## Concluding remarks

Few post-caldera volcanic crises have been monitored during their pre-eruptive phases such as at Rabaul (New Guinea) (Roggensack et al. 1996; Saunders 2001), Hudson (Chile) (Kratzmann et al. 2009; Delgado et al. 2014), Eyjafjallajökull (Iceland) (Sigmundsson et al. 2010; Tarasewicz et al. 2012), and Fernandina (Galapagos) (Chadwick et al. 2011; Bagnardi et al. 2013), and therefore, the eruptive behavior of post-caldera volcanism is not well characterized. The integration of new stratigraphic, geomorphologic, geochemical, and petrological data with a revision of chrono-stratigraphic data allowed us to decipher the evolution of Vulcanello, a post-caldera volcano of the Island of Vulcano, located along the northern part of the La Fossa caldera ring fault.

The main outcomes can be summarized as follows:

- The onset of the Vulcanello activity is not unequivocally constrained. Early eruptions of Vulcanello may have occurred in 126 or 183 BC, as reported by the Strabo and Plinius historical chronicles quoted by Mercalli and Silvestri (1891) and De Fiore (1922). The subaerial part of Vulcanello could be considered as the final part of a submarine growth process that also involved sporadic subaerial activity spaced in time.
- The subaerial volcanic activity occurred in two clusters of eruptions. The first (AD 1100 to 1250; Arrighi et al. 2006) led to the construction of the main part of the peninsula, with the growth of two cones (Vulcanello 1 and 2 lithosomes) associated with two lava flows (the Vulcanello platform lava and a submarine pillow lava field). The

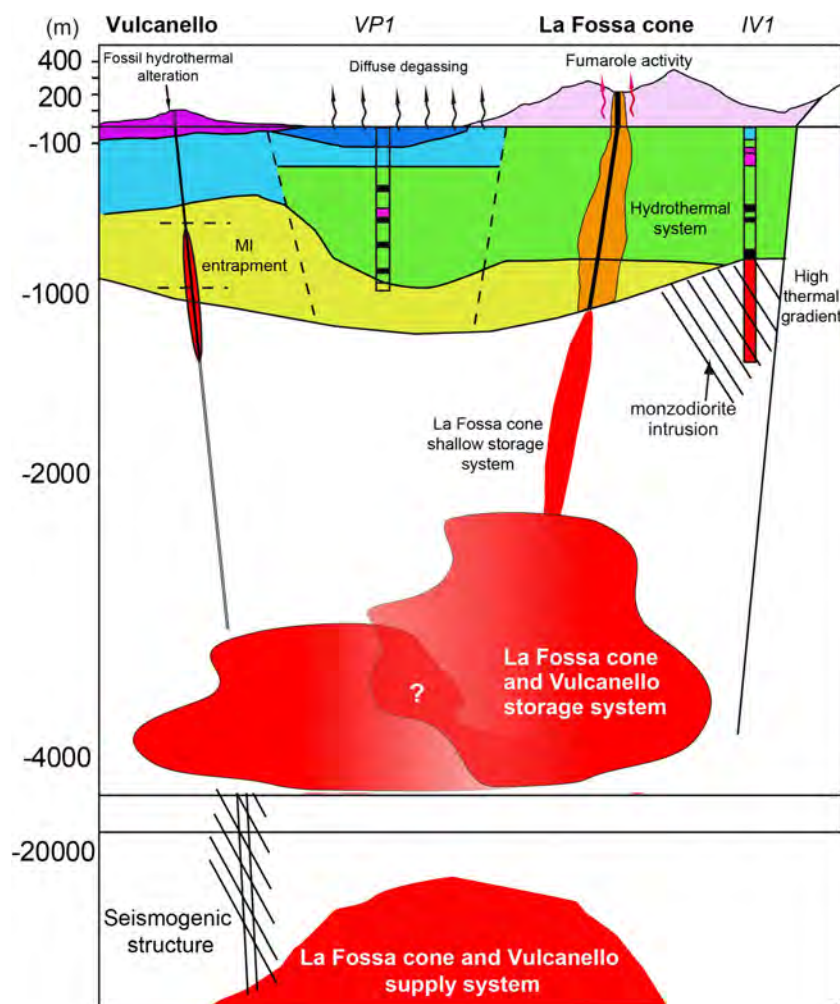


**Fig. 13** Schematic reconstruction of the Vulcanello feeding system. The presence of a magmatic chamber below the La Fossa cone is required by the diffuse degassing registered in the area and is suggested by the high geothermal gradients measured in the Agip boreholes (VP1 and IV1), pointing to magmatic temperatures at 2000–3000 m of depth. The depth of magma storage is based on different lines of evidence: (i) geophysical constraints for the lithological boundaries at depth (Chiarabba et al. 2004; Gambino et al. 2012), (ii) pressure from fluid inclusions in quartz-bearing xenoliths (Zanon et al. 2003), and (iii) minimum pressure of

crystallization from volatile content of melt inclusions in phenocrysts (Clocchiatti et al. 1994a, b; Gioncada et al. 1998). These different approaches agree in indicating a polibarcic plumbing system along the entire Vulcano history, with magma storage at about 20 km of depth, 13–8 km, 5–3 km, and a shallow storage zone at 1–2 km beneath the La Fossa cone (Peccerillo et al. 2006) and Vulcanello (this work). The short-lived very shallow storage region involved in Vulcanello activity was fed probably at the onset of Vulcanello 1 phase from a deeper reservoir along the northern La Fossa caldera ring fault

second cluster of eruptions built the third cone on the pre-existing Vulcanello 1 and 2 cones, after a period of quiescence recorded by the presence of a paleosol (0.397+0.097 ka; Keller 1980). Four EUs were produced, in association with the Roveto-Valle dei Mostri lava flows (Vulcanello 3 lithosome). The occurrence of the second cluster of eruptions is also confirmed by historical accounts (De Fiore 1922).

- The erupted volumes (DRE) of the three cones range from  $2 \times 10^{-3} \text{ km}^3$  (Vulcanello 1 lithosome) to  $3 \times 10^{-6} \text{ km}^3$  (Vulcanello 3 lithosome), while the volumes of the three lavas vary between 0.34 (submarine lava field) and  $3 \times 10^{-3} \text{ km}^3$  (Roveto lava flows). The ratio of erupted lava volume to total volume varies from 0.93

(Vulcanello 1 lithosome) to 0.99 (Vulcanello 2 and 3 lithosomes), implying that explosivity decreased through time, with the more explosive activity related to Vulcanello 1. The average growth rate of the cone in the last 1000 years is estimated  $0.28 \text{ km}^3 \text{ kyear}^{-1}$ .

- The Vulcanello activity was fed by three different magma batches. The least differentiated magmas are represented by the shoshonites erupted in Vulcanello 1 lithosome, fed by a slightly zoned magma batch, while the magmas of Vulcanello 3 were definitely the most differentiated at Vulcanello.
- The MIs from deposits of Vulcanello explosive activity record the entire differentiation history of Vulcanello magmas. The MI volatile content indicates that the

shoshonitic and latitic magmas last resided about 1 km beneath the volcano, suggesting a similarity with the La Fossa plumbing system.

- Rise of a shoshonitic magma from a deep storage system occurred at the onset of the Vulcanello eruptive activity. Magma migrated through the ring faults once magma overpressures reached 10–16 MPa along a 4–7-km-long, 43° dipping, NE–SW-oriented cone sheet. Outgassing led to mixed effusive–weak explosive activity. Considering a magma rise speed of 0.089–0.45 m/s (Vetere et al. 2007) and the length of the feeding cone sheet, we estimated an ascent time in the range of 2–22 h, in good agreement with the mixed effusive–explosive eruptive style (Scandone et al. 2007).
- The stratigraphic evidence of the contemporaneous, or almost so, activity at La Fossa cone (resurgent volcano) and Vulcanello (ring fault volcano) during the last 1000 years (Di Traglia et al. 2013) suggests the need for further investigations in order to unravel possible relationships between the different post-caldera shallow storage systems. Notably, the two post-caldera centers, fed by the same deep magmatic system (Davi et al. 2009), have, in the last 1000 years, contrasting eruptive behavior, with La Fossa producing mostly explosive eruptions, while at Vulcanello, degassed magma was generally effused. The study of MI from deposits of La Fossa eruptions that were contemporaneous or nearly so, based on stratigraphic evidence, to Vulcanello's activity will allow comparison of magma storage and ascent in the two systems, which will help us to fully understand their different eruptive behaviors. This approach (field-based volcanology joined to petrology) could give insights into post-caldera volcanism worldwide and, more specifically, support assessment of multiple-vent hazard scenarios at Vulcano.

## References

- Allard P, Behncke B, D'Amico S, Neri M, Gambino S (2006) Mt Etna 1993–2005: anatomy of an evolving eruptive cycle. *Earth Sci Rev* 78:85–114. doi:10.1016/j.earscirev.2006.04.002
- Anderson AT Jr, Newman S, Williams SN, Druitt TH, Skirius C, Stolper E (1989) H<sub>2</sub>O, CO<sub>2</sub>, Cl and gas in Plinian and ash flow Bishop rhyolite. *Geology* 17:221–225
- Arrighi S, Principe C, Rosi M (2001) Violent strombolian and subplinian eruptions at Vesuvius during post-1631 activity. *Bull Volcanol* 63: 126–150
- Arrighi S, Tanguy JC, Rosi M (2006) Eruptions of the last 2200 years at Vulcano and Vulcanello (Aeolian Islands, Italy) dated by high-accuracy archeomagnetism. *Phys Earth Planet Inter* 159:225–233
- Bagnardi M, Amelung F, Poland MP (2013) A new model for the growth of basaltic shields based on deformation of Fernandina volcano, Galápagos Islands. *Earth Planet Sci Lett* 377:358–366
- Becerril L, Galindo I, Gudmundsson A, Morales JM (2013) Depth of origin of magma in eruptions. *Sci Rep* 3:2762
- Bigazzi G, Coltelli M, Norelli P (2003) Nuove eta' delle ossidiane di Lipari determinate con il metodo delle tracce di fissione. *GeoItalia*, 4th Forum FIST, Bellaria, 16–18 September, Abstract Volume 1: 444–446
- Blanco-Montenegro I, De Ritis R, Chiappini M (2007) Imaging and modelling the subsurface structure of volcanic calderas with high-resolution aeromagnetic data at Vulcano (Aeolian Islands, Italy). *Bull Volcanol* 69:643–659
- Branca S, Del Carlo P (2005) Types of eruptions of Etna volcano AD 1670–2003: implications for short-term eruptive behaviour. *Bull Volcanol* 67:732–742
- Browning J, Gudmundsson A (2014) Ring dykes as partially captured inclined sheets: insights from field observations and numerical modelling. *EGU General Assembly Conference Abstracts* 16:415
- Bucholz CE, Gaetani GA, Behn MD, Shimizu N (2013) Post-entrapment modification of volatiles and oxygen fugacity in olivine-hosted melt inclusions. *Earth Planet Sci Lett* 374:145–155
- Carapezza ML, Barberi F, Ranaldi M, Riccia T, Tarchini L, Barrancos J, Fischer C, Perez N, Weber K, Di Piazza A, Gattuso A (2011) Diffuse CO<sub>2</sub> soil degassing and CO<sub>2</sub> and H<sub>2</sub>S concentrations in air and related hazards at Vulcano Island (Aeolian arc, Italy). *J Volcanol Geotherm Res* 207:130–144
- Caron B, Siani G, Sulpizio R, Zanchetta G, Paterne M, Santacroce R, Tema E, Zanella E (2012) Late Pleistocene to Holocene tephrostratigraphic record from the Northern Ionian Sea. *Mar Geol* 311:41–51
- Cervantes P, Wallace P (2003) Magma degassing and basaltic eruption styles: a case study of 2000 year BP Xitle volcano in central Mexico. *J Volcanol Geotherm Res* 120:249–270
- Chadwick WW Jr, Jónsson S, Geist DJ, Poland M, Johnson DJ, Batt S, Harpp KS, Ruiz A (2011) The May 2005 eruption of Fernandina volcano, Galápagos: the first circumferential dike intrusion observed by GPS and InSAR. *Bull Volcanol* 73:679–697
- Chen Y, Provost A, Schiano P, Cluzel N (2011) The rate of water loss from olivine-hosted melt inclusions. *Contrib Mineral Petrol* 162: 625–636
- Chen Y, Provost A, Schiano P, Cluzel N (2013) Magma ascent rate and initial water concentration inferred from diffusive water loss from olivine-hosted melt inclusions. *Contrib Mineral Petrol* 165:525–541
- Chiarabba C, Pino NA, Ventura G, Vilaro G (2004) Structural features of the shallow plumbing system of Vulcano Island Italy. *Bull Volcanol* 66:477–484. doi:10.1007/s00445-003-0331-9
- Cimarelli C, Di Traglia F, de Rita D, Torrente DG (2013) Space–time evolution of monogenetic volcanism in the mafic Garrotxa Volcanic Field (NE Iberian Peninsula). *Bull Volcanol* 75:1–18
- Clocchiatti R, Del Moro A, Gioncada A, Joron JL, Mosbah M, Pinarelli L, Sbrana A (1994a) Assessment of a shallow magmatic system: the 1888–90 eruption, Vulcano Island, Italy. *Bull Volcanol* 56:466–486
- Clocchiatti R, Gioncada A, Mosbah M, Sbrana A (1994b) Possible deep origin of sulphur output at Vulcano (Southern Italy) in the light of melt inclusion studies. *Acta Vulcanol* 5:49–54
- Cortese M, Frazzetta G, La Volpe L (1986) Volcanic history of Lipari (Aeolian Islands, Italy) during the last 10,000 years. *J Volcanol Geotherm Res* 27:117–133
- Davi M, De Rosa R, Donato P, Vetere F, Barca D, Cavallo A (2009) Magmatic evolution and plumbing system of ring-fault volcanism: the Vulcanello Peninsula (Aeolian Islands, Italy). *Eur J Mineral* 21: 1009–1028
- De Astis G, La Volpe L, Peccerillo A, Civetta L (1997) Volcanological and petrological evolution of Vulcano Island (Aeolian Arc, Southern Tyrrhenian Sea). *J Geophys Res* 102:8021–8050
- De Astis G, Lucchi F, Dellino P, La Volpe L, Tranne CA, Frezzotti ML, Peccerillo A (2013) Geology, volcanic history and petrology of

- Vulcano (central Aeolian archipelago). *Geol Soc Lond Mem* 37: 281–349
- De Fiore O (1922) Vulcano (Isole Eolie). *Z Vulkanol* 3:3–393
- de Rita D, Giordano G, Milli S (1998) Forestepping-backstepping stacking patterns of volcanoclastic successions: Roccamonfina volcano, Italy. *J Volcanol Geotherm Res* 80:155–178
- De Ritis R, Ravat D, Ventura G, Chiappini M (2013) Curie isotherm depth from aeromagnetic data constraining shallow heat source depths in the central Aeolian Ridge (Southern Tyrrhenian Sea, Italy). *Bull Volcanol* 75:1–11
- Del Moro A, Gioncada A, Pinarelli L, Sbrana A, Joron JL (1998) Sr, Nd and Pb isotope evidence of open system evolution at Vulcano (Aeolian arc, Italy). *Lithos* 43:81–106. doi:10.1016/S0024-4937(98)00008-5
- Delgado F, Pritchard M, Lohman R, Naranjo JA (2014) The 2011 Hudson volcano eruption (Southern Andes, Chile): pre-eruptive inflation and hotspots observed with InSAR and thermal imagery. *Bull Volcanol* 76:1–19
- Dellino P, La Volpe L (1995) Fragmentation versus transportation mechanisms in the pyroclastic sequence of Monte Pilato-Rocche Rosse (Lipari, Italy). *J Volcanol Geotherm Res* 64:211–231
- Di Traglia F, Cimarelli C, De Rita D, Gimeno Torrente D (2009) Changing eruptive styles in basaltic explosive volcanism: examples from Croscat complex scoria cone, Garrotxa Volcanic Field (NE Iberian Peninsula). *J Volcanol Geotherm Res* 180(2):89–109
- Di Traglia F, Pistolesi M, Rosi M, Bonadonna C, Fusillo R, Roverato M (2013) Growth and erosion: the volcanic geology and morphological evolution of La Fossa (Island of Vulcano, Southern Italy) in the last 1000 years. *Geomorphology* 194:94–107
- Druitt TH, Costa F, Deloule E, Dungan M, Scaillet B (2012) Decadal to monthly timescales of magma transfer and reservoir growth at a caldera volcano. *Nature* 482(7383):77–80
- Forni F, Lucchi F, Peccerillo A, Tranne A, Rossi PL, Frezzotti ML (2013) Stratigraphy and geological evolution of the Lipari volcanic complex (central Aeolian archipelago). *Geol Soc Lond Mem* 37:213–279
- Frazzetta G, Gillot PY, La Volpe L, Sheridan MF (1984) Volcanic hazards of Fossa of Vulcano: data from the last 6,000 years. *Bull Volcanol* 47:105–124
- Fulignati P, Gioncada A, Sbrana A (1998) Geologic model of the magmatic-hydrothermal system of Vulcano (Aeolian Islands, Italy). *Mineral Petrol* 62:195–222
- Gallet Y, Genevey A, Le Goff M (2002) Three millennia of directional variation of the Earth's magnetic field in western Europe as revealed by archeological artefacts. *Phys Earth Planet Inter* 131(1):81–89
- Gamberi F (2001) Volcanic facies associations in a modern volcanoclastic apron (Lipari and Vulcano offshore, Aeolian Island Arc). *Bull Volcanol* 63(4):264–273
- Gamberi F, Marani M, Savelli C (1997) Tectonic, volcanic and hydrothermal features of a submarine portion of the Aeolian arc (Tyrrhenian Sea). *Mar Geol* 140(1):167–181
- Gambino S, Milluzzo V, Scaltrito A, Scarfi L (2012) Relocation and focal mechanisms of earthquakes in the south-central sector of the Aeolian Archipelago: new structural and volcanological insights. *Tectonophysics* 524:108–115
- Geyer A, Marti J (2014) The development of ring faults during collapse caldera formation. *Front Earth Sci* 2:22. doi:10.3389/feart.2014.00022
- Gioncada A, Sbrana A (1991) La Fossa caldera, Vulcano: inferences from deep drillings. *Acta Vulcanol* 1:115–125
- Gioncada A, Clocchiatti R, Sbrana A, Bottazzi P, Massare D, Ottolini L (1998) A study of melt inclusions at Vulcano (Aeolian islands, Italy): insights on the primitive magmas and on the volcanic feeding system. *Bull Volcanol* 60:286–306
- Gioncada A, Mazzuoli R, Bisson M, Pareschi T (2003) Petrology of the post-40 ka products in the Vulcano-Lipari volcanic complex (Aeolian Islands, Italy): an example of volcanism controlled by tectonics. *J Volcanol Geotherm Res* 122:191–220
- Giordano G, De Benedetti A, Diana A, Diano G, Gaudioso F, Marasco F, Miceli M, Mollo S, Cas RAF, Funicello R (2006) The Colli Albani mafic caldera (Roma, Italy): stratigraphy, structure and petrology. *J Volcanol Geotherm Res* 155(1):49–80
- Gudmundsson A (2011) Deflection of dykes into sills at discontinuities and magma-chamber formation. *Tectonophysics* 500:50–64
- Gurioli L, Zanella E, Gioncada A, Sbrana A (2012) The historic magmatic-hydrothermal eruption of the Breccia di Commenda, Vulcano, Italy. *Bull Volcanol* 74:1235–1254. doi:10.1007/s00445-012-0590-4
- Hobden BJ, Houghton BF, Nairn IA (2002) Growth of a young, frequently active composite cone: Ngauruhoe Volcano, New Zealand. *Bull Volcanol* 64:392–409
- Intrieri E, Di Traglia F, Del Ventisette C, Gigli G, Mugnai F, Luzi G, Casagli N (2013) Flank instability of Stromboli volcano (Aeolian Islands, Southern Italy): integration of GB-InSAR and geomorphological observations. *Geomorphology* 201:60–69. doi:10.1016/j.geomorph.2013.06.007
- Keller J (1970) Die historischen eruptionen von Vulcano und Lipari. *Z Deutsch Geol Ges* 121:179–185
- Keller J (1980) The island of Vulcano. *Rend Soc Ital Miner Petrol* 36: 369–414
- Keller J (2002) Lipari's fiery past: dating the Medieval pumice eruption of Monte Pilato. International Conference UNESCO-Regione Siciliana, Lipari, September 29–October 2
- Kratzmann DJ, Carey S, Scasso R, Naranjo JA (2009) Compositional variations and magma mixing in the 1991 eruptions of Hudson volcano, Chile. *Bull Volcanol* 71:419–439. doi:10.1007/s00445-008-0234-x
- Lanza R, Zanella E (2003) Paleomagnetic secular variation at Vulcano (Aeolian Islands) during the last 135 kyr. *Earth Planet Sci Lett* 213(3):321–336
- Le Voyer M, Asimow PD, Mosenfelder JL, Guan Y, Wallace PJ, Schiano P et al (2014) Zonation of H<sub>2</sub>O and F concentrations around melt inclusions in olivines. *J Petrol* 55:685–707
- Lloyd AS, Plank T, Ruprecht P, Hauri EH, Rose W (2013) Volatile loss from melt inclusions in pyroclasts of differing sizes. *Contrib Mineral Petrol* 165:129–153
- Lowestern JB (1994) Chlorine, fluid immiscibility, and degassing in peralkaline magmas from Pantelleria, Italy. *Am Mineral* 79:353–369
- Manville V, Németh K, Kano K (2009) Source to sink: a review of three decades of progress in the understanding of volcanoclastic processes, deposits, and hazards. *Sediment Geol* 220:136–161
- Mercalli G, Silvestri O (1891) Le eruzioni dell'isola di Vulcano, incominciate il 3 Augusto 1888 e terminate il 22 Marzo 1880. *Ann Uff Centr Meteorol Geodin* 10(4):1–213
- Métrich N, Wallace PJ (2008) Volatile abundance in basaltic magmas and their degassing paths tracked by melt inclusions. In: Putirka KD, Tepley FJ III (eds) Minerals, inclusions and volcanic processes. Mineralogical Society of America, *Rev Mineral Geochem* 69:363–402
- Moore G, Vennemann T, Carmichael ISE (1998) An empirical model for the solubility of H<sub>2</sub>O in magmas to 3 kilobars. *Am Mineral* 83:36–42
- Palladino DM, Simeì S, Sottili G, Trigila R (2010) Integrated approach for the reconstruction of stratigraphy and geology of Quaternary volcanic terrains: an application to the Vulcini Volcanoes (central Italy). *Geol Soc Am Spec Pap* 464:63–84
- Parfitt EA (2004) A discussion of the mechanisms of explosive basaltic eruptions. *J Volcanol Geotherm Res* 134:77–107
- Peccerillo A, Taylor SR (1976) Geochemistry of Eocene calc-alkaline volcanic rocks from the Kastamonu area, northern Turkey. *Contrib Mineral Petrol* 58:63–81

- Peccerillo A, Frezzotti ML, De Astis G, Ventura G (2006) Modeling the magma plumbing system of Vulcano Aeolian Islands, Italy by integrated fluid inclusion geo-barometry, petrology and geophysics. *Geology* 34:17–20
- Petronis MS, Delcamp A, de Vries BVW (2013) Magma emplacement into the Lemptégy scoria cone (Chaîne Des Puys, France) explored with structural, anisotropy of magnetic susceptibility, and Paleomagnetic data. *Bull Volcanol* 75(10):1–22
- Pinel V, Jaupart C (2004) Magma storage and horizontal dyke injection beneath a volcanic edifice. *Earth Planet Sci Lett* 221:245–262
- Pistolesi M, Rosi M, Cioni R, Cashman KV, Rossotti A, Aguilera E (2011) Physical volcanology of the post-twelfth-century activity at Cotopaxi volcano, Ecuador: behavior of an andesitic central volcano. *Geol Soc Am Bull* 123(5–6):1193–1215. doi:10.1130/B30301.1
- Principe C, Tanguy JC, Arrighi S, Paiotti A, Le Goff M, Zoppi U (2004) Chronology of Vesuvius' activity from AD 79 to 1631 based on archeomagnetism of lavas and historical sources. *Bull Volcanol* 66:703–724
- Rodriguez-Gonzalez A, Fernandez-Turiel JL, Perez-Torrado FJ, Gimeno D, Aulinas M (2010) Geomorphological reconstruction and morphometric modelling applied to past volcanism. *Int J Earth Sci* 99: 645–660
- Roedder E (1984) Fluid inclusions. *Rev Mineral* 12:1–646
- Roeder PL, Emslie R (1970) Olivine-liquid equilibrium. *Contrib Mineral Petrol* 29:275–289
- Roggensack K, Williams SN, Schaefer SJ, Parnell RA (1996) Volatiles from the 1994 eruptions of Rabaul: understanding large caldera systems. *Science* 273:490–493
- Romagnoli C, Casalbore D, Bosman A, Braga R, Chiocci FL (2013) Submarine structure of Vulcano volcano (Aeolian Islands) revealed by high-resolution bathymetry and seismo-acoustic data. *Mar Geol* 338:30–45
- Rubin AM (1995) Propagation of magma-filled cracks. *Annu Rev Earth Planet Sci* 23:287–336
- Saunders SJ (2001) The shallow plumbing system of Rabaul caldera: a partially intruded ring fault? *Bull Volcanol* 63:406–420
- Scandone R, Cashman KV, Malone SD (2007) Magma supply, magma ascent and the style of volcanic eruptions. *Earth Planet Sci Lett* 253: 513–529
- Sigmundsson F, Hreinsdóttir S, Hooper A, Árnadóttir T, Pedersen R, Roberts MJ, Oskarsson N, Auriac A, Decriem J, Einarsson P, Geirsson H, Hensch M, Ofeigsson BG, Sturkell E, Sveinbjörnsson H, Feigl KL (2010) Intrusion triggering of the 2010 Eyjafjallajökull explosive eruption. *Nature* 468(7322):426–430
- Tait S (1992) Selective preservation of melt inclusions in igneous phenocrysts. *Am Mineral* 77:146–155
- Takada A (1999) Variations in magma supply and magma partitioning: the role of tectonic settings. *J Volcanol Geotherm Res* 93(1):93–110
- Tanguy JC, Le Goff M, Principe C, Arrighi S, Chillemi V, Paiotti A, La Delfa S, Patané G (2003) Archeomagnetic dating of Mediterranean volcanics of the last 2100 years: validity and limits. *Earth Planet Sci Lett* 211(1):111–124
- Tarasewicz J, White RS, Woods AW, Brandsdóttir B, Gudmundsson MT (2012) Magma mobilization by downward-propagating decompression of the Eyjafjallajökull volcanic plumbing system. *Geophys Res Lett* 39:19:1–5. doi:10.1029/2012GL053518
- Tibaldi A (2010) A new geological map of Stromboli volcano (Tyrrhenian Sea, Italy) based on application of lithostratigraphic and unconformity-bounded stratigraphic (UBS) units. *Geol Soc Am Spec Pap* 464:33–49
- Ventura G, Vilardo G, Milano G, Pino NA (1999) Relationships among crustal structure, volcanism and strike-slip tectonics in the Lipari-Vulcano volcanic complex Aeolian Islands, Southern Tyrrhenian Sea, Italy. *Phys Earth Planet Inter* 116:31–52
- Vetere F, Behrens H, Misiti V, Ventura G, Holtz F, De Rosa R, Deubener J (2007) The viscosity of shoshonitic melts (Vulcanello Peninsula, Aeolian Islands, Italy): insight on the magma ascent in dikes. *Chem Geol* 245:89–102
- Voltaggio M, Branca M, Tuccimei P, Tecce F (1995) Leaching procedure used in dating young potassic volcanic rocks by the  $^{226}\text{Ra}/^{230}\text{Th}$  method. *Earth Planet Sci Lett* 136:123–131
- Walter TR, Troll VR (2001) Formation of caldera periphery faults: an experimental study. *Bull Volcanol* 63(2–3):191–203
- Watson E B (1994) Diffusion in volatile-bearing magmas. In: Carroll, M. & Holloway, J. R. (eds) Volatiles in magmas. Mineralogical Society of America, *Rev Mineral Geochem* 30:371–411
- Zanon V, Frezzotti M L, Peccerillo A (2003) Magmatic feeding system and crustal magma accumulation beneath Vulcano Island (Italy): evidence from  $\text{CO}_2$  fluid inclusions in quartz xenoliths. *J Geophys Res* 108:2298–2301
- Zanella E (2006) Magnetic chronology in recent volcanic rocks: basic principles and case histories from Aeolian Islands. *Acta Vulcanol* 18:35–46